

AUG 22 1939

L. M. a. R.

TECHNICAL MEMORANDUMS

NATIONAL ADVISORY COMMITTEE FOR AERONAUTICS



3 1176 00121 7497

No. 903

EFFECT OF TRANSITION IN CROSS-SECTIONAL SHAPE ON THE
DEVELOPMENT OF THE VELOCITY AND PRESSURE DISTRIBUTION OF
TURBULENT FLOW IN PIPES

By Edwin Mayer

VDI-Forschungsheft 389 - Supplement to
Forschung auf dem Gebiete des Ingenieurwesens
Edition B, vol. 9, March/April 1938

FILE COPY

To be returned to
the files of the Langley
Memorial Aeronautical
Laboratory.

Washington
August 1939

144.3

1.1.2.1

1.1.3.2

NATIONAL ADVISORY COMMITTEE FOR AERONAUTICS

TECHNICAL MEMORANDUM NO. 903

EFFECT OF TRANSITION IN CROSS-SECTIONAL SHAPE ON THE
DEVELOPMENT OF THE VELOCITY AND PRESSURE DISTRIBUTION OF
TURBULENT FLOW IN PIPES*

By Edwin Mayer

I. INTRODUCTION

Very many flow processes of engineering application occur within regions where the cross sections may vary not only in area but also in shape. In the most general case the flow channel will also possess curvature so that essentially there are three factors that may be expected to affect the velocity and pressure distribution:

1. Change in the side of the flow cross section leading to a mean acceleration or retardation.
2. Curvature.
3. Change in the shape of the cross section.

Examples of flow in which these three influences operate to different degree are those in the curved intake pipes of turbines and in the impeller and guide wheels of pumps and compressors of all kinds. In order to gain insight into the difficult processes that occur, each of the three influences above must be investigated. So far, this has been done for those enumerated under 1 and 2 above. Thus Nikuradse (reference 1) and Dönch (reference 2) considered the velocity and pressure distribution in convergent and divergent channels and others, particularly Nippert (reference 3) considered curved channels of constant cross-section shape. With regard to the third factor, namely, the change in shape of the cross section

*"Einfluss der Querschnittsverformung auf die Entwicklung der Geschwindigkeits- und Druckverteilung bei turbulenten Strömungen in Rohren." VDI-Forschungsheft 389, Supplement to Forschung auf dem Gebiete des Ingenieurwesens, ed. B, vol. 9, March/April 1938, pp. 1-20.

while the area remains constant, no investigation results are as yet available.* Such an investigation will be the subject of the present paper. For this purpose it is necessary to consider the velocity and pressure relations over each entire cross section so that we are confronted with a three-dimensional problem.

II. THE TEST SET-UP

One of the most common types of transition in cross-sectional shape is that of a circle into a rectangle. Since, moreover, the built-up velocity distributions differ considerably in the flow through circular and rectangular cross sections, it may be expected that the effect of the change in cross section on the velocity and pressure relations will show up very strongly. For this reason, there is considered in this paper the flow where the shape of cross section changes from circle to rectangle or in the reverse direction, from rectangle to circle. The tests were carried out with air as the medium.

Figure 1 shows the test set-up for the investigation of the velocity and pressure distributions in the transition from a circular cross section (diameter, 190 mm) into a rectangular one of the same area (width, 238 mm; height, 119 mm). These relatively large cross-sectional areas were chosen in order that the percent change in cross-section area resulting from the insertion of the velocity- and pressure-measuring apparatus should be as small as possible and thus the actual velocity and pressure distributions measured with the greatest possible accuracy. The tests were performed in the open air. With the intake chamber *k* not connected to the pipe the readings of the micromanometers which served to measure the velocity and the pressure were subject to rather large irregular fluctuations on some days as a result of wind impact on the open pipe. In order to eliminate this difficulty in the reading of the instruments, an intake chamber *k* of approximately 2 cubic meters volume was joined to the end of the pipe. The bottom of the chamber is formed of two sheet-metal layers ¹ hav-

*One of the few suggestions for the necessity of taking into account the effects of change in cross-sectional shape on the development of the velocity distribution is found in the dissertation of E. Schröder (reference 4).

ing orifices through which the air is sucked in, the chamber being otherwise completely closed. To avoid disturbances resulting from jet contraction and formation of vortices at the sharp pipe edges at the inlet to the entry run of pipe a, an entry throat e is inserted between the intake chamber and the circular pipe through which throat the air in the intake chamber is gradually accelerated.

In the preliminary tests, it was found that the velocity profile at the entry run of pipe was asymmetrical to the pipe axis, more air flowing through the upper or lower part of the circular section, depending on the distance of the profile from the pipe inlet. In order to avoid this, two honeycombs g, one directly behind the throat and the other 5 meters distant, were installed in the pipe a. They consist of thin-walled sheet metal tubes of about 250-millimeter length and 25-millimeter diameter arranged to fill out the cross section by honeycombs. The installation of these resulted in symmetric velocity distribution with respect to the pipe axis.

The entry run of pipe was 17 meters long, that is, about 90 diameters. The pipe is formed of an 8-meter length of normally welded sheet metal while the remaining length of 9 meters was of seamless, drawn sheet brass.

Preliminary tests were at first necessary in order to see whether the entry run of 90 diameters was sufficient to give at its end a built-up turbulent velocity profile. The condition for this stable velocity profile is that it no longer changes with increase in entry length. According to investigations by Kirsten (reference 5), the length of pipe chosen is sufficient to give a stationary, turbulent velocity profile. In the present case, because of the asymmetrical entry, the possibility arose that these disturbances might require a longer entry run of pipe.

An accurate velocity profile was therefore taken at the end of the entry run, that is, after a length of 90 d and also one after a length of 80 d. Comparison gave an accurate agreement between the two velocity distributions. A further proof that the length of entry run was sufficient will be provided in the more detailed discussion below of the initial profile (section VI). It is essential to have a stationary velocity profile at the end of the entry run in order to obtain independently the effect of the change in cross section on the velocity and pressure distributions

and avoid disturbances that may be ascribed merely to a short length of pipe. It must be noted, however, that the requirement of a built-up turbulent velocity profile at the beginning of the transition section very seldom is met with in practice where such transitions in cross sections occur. It is necessary, however, to assume such built-up profiles in systematic tests in order to be able to simplify to some extent the difficult relations involved. Only then will it be possible to consider measurements with other entry profiles that occur more in practice.

At the end of the entry run of pipe, there is the transition piece *v* which permits the transition from the circular cross section to the rectangular while maintaining the area the same. In order to be able to follow further the development of the velocity and pressure distribution after the exit of the air from the transition piece and to eliminate disturbing reaction effects on the velocity and pressure distribution in the transition piece itself the air after leaving the transition piece flows into a 5 meters long rectangular exit run *b*. The construction of the latter may be seen from figure 2 which shows a section of it. It is assembled from 3 millimeters thick smooth sheet brass and rests on the cast iron frames *r* which are screwed on at a distance of 1 meter apart on two U beams *s*. In order to obtain sharp edges the two latter sheets *sb* are welded to the base plate *bb* and screwed together with the cover plate *db*. The exit run *b* ends in a deflecting chamber *u* (fig. 1) out of which the air is sucked by a blower.

The test set-up for the flow in the opposite direction where the cross section changes from rectangular to circular of equal area is shown in figure 3. The entry run of pipe *a* connected ahead of the transition piece *v* has a length of $11 \text{ m} = 70 d_h$ (d_h = hydraulic diameter $= \frac{4F}{U}$ = 0.1586 m, F = area of section, U = perimeter of cross section), whereas the connecting exit run *b* of circular section is again 5 meters long. In order to avoid disturbances, there is in this case, too, at the entrance to the entry run an entry throat *e*.

In the case of the flow direction rectangle \longrightarrow circle there is also to be investigated the development of the velocity distribution along the entry run itself, no measurements of this kind having so far been published according to the author's knowledge. In order to carry out

these measurements it was necessary to dispense with the intake chamber ahead of the entry throat since because of the deflection of the intake air this chamber would have made the velocity profile in the first part of the entry run asymmetrical so that the development of the velocity profiles could not be followed. Similarly, it was also necessary to dispense with a honeycomb in the entry length of pipe since it would give rise in part of the pipe to a velocity distribution that would not agree with that of the same section without the honeycomb. It was all the easier to dispense with the honeycomb as it was found that in the initial rectangular run of pipe there appeared no tendency toward a velocity distribution asymmetrical with respect to the axis. On account of the absence of the intake chamber, the tests for the flow direction rectangle \longrightarrow circle were carried out only on calm days.

As in the case of the transition circle \longrightarrow rectangle it also was established for the reverse direction whether the chosen length of pipe was sufficient for attaining a fully built-up turbulent velocity distribution. As may be seen from figure 7, a stationary built-up turbulent velocity distribution is attained at the very entrance to the transition piece, so that the length of the initial run of pipe is sufficient.

The remaining construction of the test set-up corresponds to the transition circle \longrightarrow rectangle. The air flows out of the transition piece *v* through the circular exit run *b* into the deflecting chamber *u* out of which it is sucked by the blower and is again discharged into the free atmosphere. The purpose of the Prandtl tube *p* indicated in figures 1 and 3 will be discussed in section V.

III. THE VELOCITY AND PRESSURE-MEASURING APPARATUS

For the measurement of the velocity and pressure distributions in the different cross sections a pressure sphere whose construction and principal dimensions may be seen from figure 4 was made use of. The entire apparatus rests on a base plate *g* which is screwed on to the pipe over the measuring orifices (*s* in fig. 8) to be further described below. (The manner of this attachment may also be seen from fig. 11.) On the base plate *g* is a cylinder *w* rotatable in a plane in both directions and to this is attached the support *h* of the shaft of the sphere.

The magnitude of the angle of rotation $\pm \psi$ of the cylinder with respect to the vertical position is read off on a graduated circle m . The shaft s of the sphere is axially displaceable in the support and can be turned about its axis (angle of rotation α). At the upper end of the support is the headpiece o rotatable in the support, ground smooth on one side and provided with a vernier scale n . Through this the sphere shaft, which is provided with a mm scale along its length is visible so that the depth of lowering of the pressure sphere into the transition section may be determined. At the upper end of the shaft there is a disk r rotating with it and provided with a graduated circle on which the angle of rotation $\pm \alpha$ of the shaft with respect to a determined zero position may be read off by rotating the pointer z over the disk until the reflection of the tip of the pointer coincides with the pointer tip z_1 over the mirror sp .

By adjusting the angle ψ and the lowering depth, all points of the lower half and a portion of the points of the upper half of each section of the transition piece may be reached. The sphere k itself has four pressure orifices (fig. 5a) in contrast to the spheres that have so far been employed in the Karlsruhe Laboratory for flow machines, where 12-millimeter diameter spheres provided with five pressure orifices are employed. (fig. 5b). A detailed description of a pressure sphere with five orifices may be found in the paper by Krisam (reference 6) so that an explanation of the principle of the measurement of velocity and pressure with the aid of the sphere may be dispensed with here. A deviation was made from the usual type of construction in order that a smaller sphere diameter may be obtained. With the sphere diameter chosen of 8 millimeters, it is no longer possible to weld securely and air tight the five small pressure tubes required for a sphere with five orifices (0.8 mm outer diameter, and 0.5 mm inner diameter) that serve to convey the pressure through the sphere shaft. In order to keep the diameter of the sphere down to 8 millimeters and at the same time to maintain the dimensions of the pressure tubes, there is no choice than to attempt to construct a practical instrument with fewer than five orifices which should permit the measurement of the velocity in magnitude and direction as well as of the pressure. In using the 8-millimeter sphere with four orifices, it is necessary, because of the elimination orifice 3 (fig. 5b) to define the coefficient k_8 for the determination of the angle δ (angle between the velocity direction and the perpendicular to the sphere shaft in the

meridian plane which contains the orifices 1 and 2) differently than that for the sphere with five orifices. In our case

$$k_{\delta} = \frac{k_2 - k_1}{k_2 - k_4} = \frac{h_2 - h_1}{h_2 - h_4}$$

where k_1 , k_2 , and k_4 are nondimensional coefficients whose values must be determined by calibration from the relation

$$k_{1,2,4} = (h_{1,2,4} - p/\gamma) 2g/c^2$$

as a function of δ . (h_1 , h_2 , h_4 are the pressure heads at orifices 1, 2, and 4; p is static pressure; γ , specific weight of the flow medium; g , acceleration of gravity; c , velocity of flow.) The k_{δ} curve plotted against $+\delta$ and $-\delta$ must be of such a form that to each value of k_{δ} there corresponds a definite angle and not several values of δ . In order to satisfy this condition, the orifice 2 on the sphere was somewhat inclined toward the shaft so that the axis of the orifice forms an angle of 6° with the middle plane of the sphere at right angles to the shaft axis. For the same reason, the orifice 1 assumed a somewhat different position, its axis forming with the middle plane an angle of 30° (fig. 5a). In this way there was obtained a unique curve for k_{δ} as a function of the angle $\pm\delta$ as is shown in the calibration curve of figure 6 for the values of δ between $+35^\circ$ and -35° . For values of δ larger than $\pm 35^\circ$, the k_{δ} curve becomes many-valued. In this range therefore, the pressure sphere is no longer applicable. In the case of the tests under consideration, however, no such large values of δ were to be expected.

In the measurement of the velocity and the pressure at any position with the aid of the pressure sphere apparatus, the procedure is as follows. After adjustment of the sphere coordinates of the corresponding measuring station, that is, the lowering depth of the shaft and the angle $\pm\psi$, that sphere is rotated until the pressure at orifice 4 becomes equal to that at orifice 5. On the scale attached to the sphere shaft, this angle of rotation $\pm\alpha$ can then be read off. The zero line for measuring the angle α lies on the line of intersection of the plane of the disk and the meridian plane of the sphere through the orifices 1 and 2. After the determination of the value of k_{δ}

from the manometer readings h_1 , h_2 , and h_4 by the relation given above, there is determined from the calibration curve the angle $\pm\delta$ corresponding to this value of k_8 . There are furthermore obtained from the calibration curve the velocity coefficients k_1 and k_2 . The speed and pressure energy is then obtained from the relations

$$\frac{c^2}{2g} = \frac{h_2 - h_1}{k_2 - k_1} \quad \text{and} \quad \frac{p}{\gamma} = h_1 - k_1 \frac{c^2}{2g}$$

The velocity c thus determined is split up into three components c_x , c_y , and c_z at right angles to one another. The c_z component is parallel to the longitudinal axis of the test length and is considered positive in the direction of the main flow. In the plane at right angles to it are the c_x and c_y axes. Their positive sense is taken in the usual manner so that the rotation from the positive c_x axis to the positive c_y axis gives a right hand screw direction to the positive c_z axis. From the measured angles α , δ , ψ , and the determined velocity c , the velocity components are computed from the relations

$$c_x = c(\cos \delta \sin \alpha \cos \psi - \sin \delta \sin \psi),$$

$$c_y = -c(\sin \delta \cos \psi + \cos \delta \sin \alpha \sin \psi),$$

$$c_z = c \cos \delta \cos \alpha$$

Concerning the effect of the shaft of the sphere on the velocity measurement, the following may be remarked. In the most unfavorable case, that is, in the measurement of the velocity at the lowest measuring positions of the circular cross section of the transition pieces, the 9-millimeter diameter shaft obstructs the cross section over a length of approximately 180 millimeters. This means therefore a reduction in area of the total section of about 16.2 cm², which is 5.6 percent. The sphere was calibrated by the method described in detail in the paper by Krisam (reference 6) and also for a circular pipe of 190-millimeter diameter, the shaft extending 55 millimeters into the cross section. The comparison velocity and comparison pressure were measured with a Prandtl tube whose shaft extended diametrically opposite the sphere also 55 millimeters into the cross section. The distances of the pressure slot and the dynamic pressure orifice from the shaft of the Prandtl tube correspond to that required in the Handbuch der Experimental Physik (reference 7). The dimensions there in-

licated are such that the effect of tube shaft on the measurement of the dynamic and static pressures is eliminated and there may thus be obtained the true velocity at a point. It is of importance to see that in the calibration of the sphere apparatus there should be a similar decrease in area by $10 \text{ cm}^2 = 3.5 \text{ percent}$. The effect of the sphere shaft on the velocity measurement therefore involves in the most unfavorable case a decrease in area of 6.2 cm^2 . In order to test the effect of this the velocities in the pure circular cross section were measured first with the sphere and then with a small pitot tube of 2 mm shaft diameter. The two velocity distributions thus obtained show a very good agreement from which it may be concluded that the effect of the sphere shaft on the velocity measurement is negligible. Also the pressure measurement carried out with the aid of the sphere gave for each point of the circular cross section the same pressure and hence led to the conclusion that the shaft of the sphere is also without effect on the pressure measurement. As mentioned in the paper by Krisam the sphere gives erroneous values in the neighborhood of the wall. The velocities and pressures are measured too high there and the measurements of the angles also disagree.

The causes for these errors are first, the fact that the velocity distribution in the neighborhood of the wall is disturbed by the sphere and particularly the fact that the sphere is located in a region of large velocity drop, so that very different velocities are found at each of the orifices of the sphere. At such points therefore the velocities were measured with a small pitot tube (fig. 7), the static pressure being taken at the same time at the pressure orifices at the wall. Also in the measurement of the velocity in the neighborhood of the wall in those cross sections in which the pressure varied over the periphery of the cross section of the static pressure of the wall orifice was differentially connected to the dynamic pressure at the other end of the micromanometer and then the reading measured with the sphere instrument, corrected to the corresponding actual static pressure at the point under consideration. In the measurement with the pitot tube, the latter was placed in the support in the position of the sphere shaft. In order to be able to measure the velocity in the same plane, the pitot tube was bent in the form of a hook. With this instrument, it is possible to take velocity measurements at points having a minimum distance from the wall of $1\text{-}1/2 \text{ mm}$. As an indication of the accuracy of the velocity measurements, it may be said that the discharge V given by the continuity law $V =$

$F c_{zm}$ (c_{zm} is mean velocity through section) at the various measuring sections F gave the same value with a deviation of ± 0.75 percent.

IV. THE TRANSITION PIECES

Two transition pieces were investigated. Both have the following principal dimensions as may also be seen from figures 8 and 9:

Diameter of circular section: 190 mm

Rectangular section: 238 x 119 mm²

The transition length, that is, the distance between the fully built-up circular and rectangular sections, amounts in the case of the first transition piece I to 440 millimeters and in transition piece II to 110 millimeters.

A circle may be deformed into a rectangle of the same area along a straight axis in an infinite number of ways. From the condition, however, that there is a flow medium through the sections the number of possible deformations becomes strongly limited. The main condition to be satisfied by the transition piece is that the transition be uniform and continuous along the entire length, that is, that it follow a definite law of deformation, so that there be no discontinuities in the transition from one section to the other and each intermediate section possess the same area.

The transition length for piece I is so chosen that the angles between the axis and the walls of the transition piece remain below 5° . On the other hand, the angles of transition piece II, on account of the shorter length, may reach a value up to 19° . The latter transition piece was mostly for the purpose of investigating whether, because of local negative accelerations, separation from the wall occurs in spite of a constant mean velocity. The law of deformation according to which the circle is transformed into the rectangle will be explained with the aid of figure 10.

There are first shown the initial and end cross sections. It is readily seen that the vertically hatched areas 2A subtracted from the circle are equal to the hori-

horizontally hatched areas 2B added to the rectangle. Seven intermediate cross sections are indicated for forming the transition piece. The contours of these sections were obtained in the following manner. Areas A and B were divided into eight equal partial areas as shown in the figure. The lines joining the corresponding division points give the contour of an intermediate cross section (fig. 10, where this construction is shown for the middle cross section 5). The partial areas subtracted at the upper and lower sides are added laterally to the circle, so that each intermediate section has the same area as the initial and end section of the transition piece. The sections finally obtained are shown in figure 8 with the only difference that the edge arising at E is somewhat broken, the areas, of course, still remaining the same.

The transition pieces were cast of silumin since the latter gives a very smooth surface and retains its shape very well. Both of these properties must unconditionally be required of the material used for the casting since it is subsequently impossible to work the inner surfaces of the transition piece, the surfaces being merely smoothed over with glass paper. On the upper sides of the transition pieces are cast the seats a (figs. 8 and 9) to which the velocity apparatus may be screwed on and extended through the milled slots s at the various cross sections. The slots of those cross sections at which no measurements were taken were made airtight by accurately cast lead covers. At the ends of the transition pieces themselves are the initial and end cross sections 200 millimeters apart, so that transition piece I has a total length of $400 + 2 \times 200 = 840$ millimeters and piece II a length of $110 + 2 \times 200 = 510$ millimeters. Transition piece I is provided with 11 measuring sections and hence with 11 seats with slots, whereas transition piece II possesses five measuring sections. Laterally and at the under sides there are located "eyes" au at each second section of piece I and at each section of piece II, which are provided with orifices b and tubes t for taking the static pressure in measuring the velocities in the neighborhood of the wall with the aid of the pitot tube.

It was first necessary to test the cast transition pieces for their suitability for the tests under consideration. It was particularly necessary to investigate whether the required cross sections agreed with those of the actual transition pieces and whether the area was constant as required. For this purpose each cross section of

the transition pieces was measured and plotted with the aid of a caliper instrument. This instrument consisted of a pointed metal rod st which is inserted in the support h of figure 4 in place of the sphere shaft s , figure 11. It is then possible to measure the lower and a portion of the lateral parts of the cross sections accurately by reading the angle with the scale m and the depth of insertion of the rod. To measure the portion of the cross sections not reached with the straight rod, there is provided a hooked point sp as shown in figure 11. The areas of the sections thus measured out and plotted were obtained by a planimeter and are given in tables 1 and 2. The cross sections of the circular and rectangular entry and exit runs all had an area of 283.0 cm^2 . As may be seen from the above tables the maximum deviation from the required area ($F = 283.0 \text{ cm}^2$) was about 5 cm^2 , which corresponds to an error of 1.8 percent. These inaccuracies must be reckoned with since hardly any greater accuracy could be expected with the pieces thus roughly cast and not worked over.

5. THE TEST PROCEDURE

Corresponding to the normal output of the blower, the tests for the two transition pieces investigated were carried out for a Reynolds Number of about $R = 192,000$, the latter being computed in the case of the transition circle \longrightarrow rectangle for the fully built-up circular cross section with diameter $d = 0.190 \text{ m}$ and for the transition rectangle \longrightarrow circle for the fully built-up rectangular cross section with width $b = 0.238 \text{ m}$ and height $h = 0.119 \text{ m}$. Corresponding to this circle diameter and the hydraulic diameter d_h computed from the relation $d_h = 4 F/U = 0.1586 \text{ m}$ ($F = \text{area}$ and $U = \text{wetted perimeter of the section}$) there is obtained for approximately equal Reynolds Number $R = c_{zm} d/\nu$ or $R = c_{zm} d_h/\nu = 192,000$ for the transition circle \longrightarrow rectangle a mean air velocity of $c_{zm} = 14.0 \text{ m/s}$ and for the transition: rectangle \longrightarrow circle $c_{zm} = 16.3 \text{ m/s}$. The kinematic viscosity ν of the air was assumed to be $13.6 \times 10^{-6} \text{ m}^2/\text{s}$.

In order to have a measure for the quantity of air

discharged there is a Prandtl tube p located at the sections shown in figures 1 and 3 in the pipe axis. It was found by velocity measurements in section 10 that this apparatus for normal discharge of air for the case of the transition circle \longrightarrow rectangle shows a velocity of 17 m/s and for the transition rectangle \longrightarrow circle a velocity of 20.3 m/s. In view of the small size of the direct current rectifying network from which the motor driving the blower was fed, the rotational speed depended on the loading network, so that at irregular time intervals different velocities with different discharge quantities were obtained which remained constant for some length of time. In order therefore to obtain a constant air flow for determining the velocity and pressure distribution in a section of the transition piece, it would have been necessary to vary the field of the motor by a resistance to correspond with the change in rotational speed. In order to avoid the need for this continuous regulation, the velocity and pressure measurements were carried out by the following method.

In measuring the velocity c and the pressure p at any point with the aid of the pressure sphere the velocity c_{st} was recorded with the aid of the Prandtl comparison instrument simultaneously with the three micro-manometers giving the pressure heads at the orifices 1, 2, and 4. A ratio c/c_{st} may be determined directly from this measurement. By checking, it was found that this ratio c/c_{st} gives for a definite measuring point a value which is constant for discharge quantities that are about 10 percent higher or lower than the normal discharge quantity. Similar velocity distributions were thus obtained for all point at which the velocity was measured with the sphere. Also, for the points in the neighborhood of the wall where the velocity was obtained with a pitot tube c/c_{st} was obtained as a constant ratio for the same point, so that it may be said that the velocity profiles at the measuring planes of each cross section remained similar in spite of the change in the Reynolds Number in the given region. To determine the velocity distribution at the various cross sections, the ratio c^2/c_{st}^2 or, taking the square root, c/c_{st} , was therefore directly determined from the monometer readings for the measuring point under consideration. From this was obtained the absolute value of the velocity for constant mean velocity c_{zm} for the transition circle \longrightarrow rectangle, according to the relation $c = 17 c/c_{st}$; for the transition rectangle \longrightarrow circle the relation is $c = 20.3 c/c_{st}$.

For determining the pressures, three pressure and velocity measurements for three different discharge quantities were taken at each measuring point. The speed of the motor was so regulated that the blower first drew in the normal quantity of air and then quantities 10 percent higher and lower, respectively. Corresponding to the values of $c_{st}^2/2$ g in mm water, the pressure heads were measured with the sphere and graphically plotted. This gave for all measuring points a straight line. Taking into account the atmospheric pressure prevailing on the day of the test and the moisture of the air and its temperature, the reading corresponding to the normal air quantity for $c_{st}^2/2$ g in mm water was computed from the following relations. In the transition circle \longrightarrow rectangle, the velocity head of the tube corresponding to the normal discharge $c_{st}^2/2$ g = $17^2/2$ g = 14.75 m air column.* This value, recomputed from the relation

$c_{st}^2/2$ g = 14.75 $\times 1000 \frac{\gamma_L}{\gamma_W}$ gives the required dynamic

pressure for that particular day at the Prandtl tube in mm water for the normal quantity of air flowing through the pipe (γ_L = specific weight of the air, γ_W = specific weight of the water). It is then possible to obtain the pressure in mm water from the graph. This pressure must be converted in meters of air from the relation $p/\gamma_L =$

$p/\gamma_W \frac{\gamma_W}{\gamma_L 1000}$ since only the pressure head expressed in

meters of air column measured at the same point on days with different γ_L gives a constant value. The same computation procedure was applied to the transition rectangle \longrightarrow circle for a velocity head $c_{st}^2/2$ g = $20.3^2/2$ g = 21.1 m air column for the determination of the pressure. This method of measuring the pressure has yet another advantage in that it provides for each measuring point a mean value from the three readings for the determination of the angles and the ratio c/c_{st} and so the constantly occurring small reading errors cancel.

With regard to the location of the measuring points at each of the cross sections, it is to be observed that

*For these small pressures, it is convenient to indicate the data in meters air column.

they all lie on parallels to two perpendicular axes. The axes are the lines of symmetry of each cross section, their position being determined from the cross section contours found with the aid of the caliper apparatus. The number of measuring points was chosen in such a manner that at positions with rather flat velocity profiles, that is, small velocity drops, the distance between the measuring points amounted from 1.5 to 2 mm. In those parts of the cross sections where secondary flows were to be expected, the distance between the points was made smaller. As an example, figure 12 gives the arrangement for the lower halves of sections 0 and 10.

With regard to the numbering of the straight lines parallel and at right angles to the axes, it is to be observed that at each cross section lines having the same distance from the axes are assigned the same number and therefore all lie in the same measuring plane which is parallel to the principal axis of the transition piece and at right angles to one of the two axes of each cross section. The letter a following a number indicates that this line is 5 mm distant from the line having that number. Thus, for example, the measuring line 1a is 5 mm from the line 1. The letter b indicates a distance of 10 mm and c a distance of 15 mm. Lines with two successive numbers and no letters have a distance of 20 mm apart.

In the tests the result was found that in each section both for the transition circle \longrightarrow rectangle and rectangle \longrightarrow circle the velocities occurring at all attainable measuring points were exactly as large as at those symmetrically located with respect to them in another quadrant of the cross section. Only at the measuring points very near the location of the measuring apparatus did small deviations appear. Also with respect to the velocity directions no essential differences could be established in the various quadrants of the cross sections. In several intermediate cross sections therefore, only the velocity and pressure distribution in one fourth of the cross section was measured and the symmetry checked by random tests. For this reason, in presenting the test results in the following sections, only the velocity distributions for a fourth of the cross section will be given.

VI. THE INITIAL PROFILE IN CROSS SECTION 10 OF THE
 TRANSITION PIECE FOR THE FLOW DIRECTION
 CIRCLE \longrightarrow RECTANGLE

The velocity profile for the circular cross section 10 in the flow-direction circle \longrightarrow rectangle denoted in what follows by C \longrightarrow R(I) and C \longrightarrow R(II) is the same for all radial planes of the two pieces and thus possesses rotational symmetry. The profile is shown in figure 13. It was proven that this profile represents the fully developed turbulent condition. In order to make a comparison with the measurements of other authors, the velocity distribution was checked, using the Prandtl mixing length relation (reference 8)

$$l = \sqrt{\frac{\tau}{\rho} \frac{dc_z}{d\eta}}$$

(l , mixing length; $\rho = \gamma/g$, density). Taking into account the linear drop of the shear stress τ as a function of the distance η from the wall according to the relation

$$\frac{\tau}{\tau_0} = \frac{r - \eta}{r}$$

(τ_0 , shear stress at the wall; r , pipe radius) and substituting the pressure drop in the direction z of the pipe axis into the relation

$$\tau_0 = \frac{r}{2} \frac{dp}{dz}$$

there is obtained the distribution of the mixing length shown in figure 14. For the distribution of the mixing length, Prandtl gives the following formula

$$\frac{l}{r} = 0.14 - 0.08 \left(1 - \frac{\eta}{r}\right)^2 - 0.06 \left(1 - \frac{\eta}{r}\right)^4$$

In comparing the values of l/r , computed from the above formula with those found from the measurement, very good agreement is obtained.

If it is desired to give the velocity distribution directly by means of an exponential law of the form $c_z/c_{st} = a \eta^{1/n}$ (a is constant; η , distance from the wall; $1/n$, exponent), the logarithm of c_z/c_{st} is plotted against the distance from the wall as abscissa and the exponent $1/n$ found, in the usual way, as shown in figure 15. (In order to obtain positive values, the arguments of the ordinates are multiplied by 10.) From the slope of the straight line in figure 15, which is drawn from the initial profile of figure 13, the value of the exponent may be directly obtained as $1/n = 1/8.3$. This value, too, agrees well with the measurements of other authors.

That both the mixing-length distribution and the exponential law agree with the measurements of other experimenters is another confirmation of the fact that at the entrance to the circular cross section of the transition piece, the turbulent velocity profile is fully built up. In addition, the conclusion may be drawn that the transition has no effect on the velocity distribution in section 10.

VII. THE FLOW IN THE ENTRY RUN OF RECTANGULAR SECTION

As already mentioned, in the case of the transition rectangle \longrightarrow circle, denoted in what follows by $R \longrightarrow C(I)$ and $R \longrightarrow C(II)$, it was first necessary to establish whether at the entrance to the transition piece there was a fully built-up turbulent velocity distribution. For this purpose it was necessary to obtain the velocity distribution in several cross sections of the entry run of pipe in order to see from the comparison whether and where a position occurred from which position on the velocity distribution over the entire cross section no longer varied, that is, whether the initial run of pipe was long enough. For the sake of completeness and in view of the lack of such measurements in entry runs of rectangular cross section, the velocity profiles were measured along the entire length of the run at the sections indicated in figure 16, the measuring apparatus used being the pitot tube of figure 7. The attempt to use the sphere apparatus encountered difficulties since the fluctuations of the fluid columns in the three micromanometers, particularly in the measurement of the cross sections with short entry runs, were so large that the readings became too inaccurate.

As a result of the difficulties, considered more in detail in section VIII, which arose in following the development of the velocities in a spatial flow, it was found best also in this case to present the conditions in the various cross sections in the form of "isotachs" (c_z/c_{st} or $c_z/c_{max} = \text{constant}$). The measured velocity profiles in cross section 0 may be seen on figure 17 whereas the isotach diagrams for all cross sections indicated in figure 16 are given in figures 18 to 26.

It may be seen that at cross section I nearest the entrance (fig. 18) there is a sufficiently uniform velocity distribution over the entire cross section with a rapid drop toward the wall as may also be expected by analogy with the tests of Kirsten (reference 5) in entry runs of circular cross section. For after such a short path of $1.55 \text{ m} = 9.5 d_h$ in the pipe the particles of air further removed from the bounding walls are not yet affected by the shear stress in the neighborhood of the wall. In cross section II (fig. 19) there will be found, though only in a small region in the direct vicinity of the edges, that behavior first established by Nikuradse (reference 9) for the built-up turbulent flow in rectangular pipes. From this phenomenon, according to which at some positions particles farther removed from the wall have smaller velocities than those closer to the wall, Nikuradse derived the conclusion that in turbulent flow in pipes of noncircular cross section secondary flows are superimposed on the main flow. An explanation for the origin of such secondary flows at the edges of a cross section has been given by Prandtl (reference 8) which will be briefly reviewed here. Prandtl concludes from the above-mentioned facts that in the case of turbulent flow, there exists, in addition to the to-and-fro motion in the direction of maximum velocity drop, a still stronger to-and-fro motion at right angles to it, that is, in the direction of the isotachs. If this is the case, then it immediately follows that centrifugal forces thereby arise on the particles which move up and down along the curvatures of the isotachs. These forces always point toward one direction, namely the convex sides of the isotachs and are stronger the greater the curvature of the latter. The result is that the particles move outward along the angle bisectors of the corners of the cross section whereby the particles located at the corners are forced, for reasons of continuity, to deviate first laterally and then inwardly (see fig. 27). Since the particles flowing toward the corners possess a relatively large axial velocity, whereas conversely, the outwardly

flowing particles as a result of the friction at the wall have a smaller axial velocity, this explains the unexpected appearance of the velocity profiles and hence the isotachs. The question as to the reason for the turbulent to-and-fro motion in the manner described is not answered by this consideration of Prandtl as it leads to the more comprehensive question of the origin and inner mechanism of turbulence in three dimensional flows and this in the present stage of our turbulence investigation must still remain unanswered.

Returning to the consideration of the development of the isotach curves in the entry run, it may be found in cross section III (fig. 20) that the strong indentations of the isotachs at the positions where the particles are pushed inward have entirely disappeared. On the basis of the Prandtl theory, this phenomenon may be explained by the consideration that the particles with relatively smaller axial velocities with increasing pipe length are pushed aside into the interior of the flow and replaced by particles which have larger axial velocities. In cross section IV (fig. 21) the secondary flow has taken in a greater region at the edge so that at points whose distance is about 20 mm from the wall the effect is already evident. The particles with relatively smaller velocities pushed toward the interior of the cross section apparently gradually give rise to the indentation of the isotachs that heretofore were not affected by the secondary flow, so that by the decrease in the radius of curvature the secondary flow may also be built up there. This process continues (see cross section V, fig. 22) until all instabilities in the flow have disappeared. It is in cross section O (fig. 26) that the built-up turbulent velocity distribution is first found, there being superimposed over the entire flow secondary flows that include a large region of the cross section. As may be seen from the built-up isotach curves at a section with shorter entry run, there is no isotach picture that entirely coincides with that of section O, so that the correctness of the statement that the profile of section O represents the fully built-up turbulence still remains to be proven. This proof may be given as follows: At the entrance to the initial run there was built in a honeycomb similar to that in the circular initial run in the transition circle \longrightarrow rectangle. In this manner the required initial run was shortened, so that in section VII a velocity distribution could be established which no longer varied with increasing length of run and which agrees with that of cross section O measured without honeycomb.

For a further characterization of the velocity development along the entry run without honeycomb, there was plotted the ratio of the mean velocity to the maximum in the pipe axis as a function of the length of run. (See fig. 28.) As shown by the figure, this ratio drops sharply from the value $c_{zm}/c_{max} = 1.0$ at the beginning of the run and this corresponds to equal velocity over the entire cross section and then attains in cross section II and in the following cross sections up to section VI, so long as the secondary flows are restricted to the corners, an almost constant value. From section VI on, the secondary flow gives rise to a change in the maximum velocity until the latter maintains a constant value from section VIII on. The first change in the ratio c_{zm}/c_{max} is thus essentially produced by the pure friction effects at the wall whereas the subsequent lowering of this ratio may be ascribed to the effects of the turbulence of the flow.

In order to check whether the velocity distribution, also, at least in the neighborhood of the walls of the individual cross sections of the entry run, may be expressed by a simple exponential law of the form $c_z/c_{st} = a \eta^{1/n}$ (where η is the shortest distance from the wall), there was plotted by the method already described in section 6 (fig. 15), for all the measured profiles in the measuring planes indicated in figure 12, the logarithm of $10 c_z/c_{st}$ against the logarithm of the distance from the wall (fig. 29). In most cases a straight line could be drawn through the points thus obtained and the existence of a law of the above simple type established. The values of n for the different profiles are given in table 3. Most of the values there indicated are valid up to a distance from the wall of 15 millimeters. With increasing length of entry run, the velocity distribution is well represented by these values for an increasingly larger region of the cross-section area. The dashes in the table in the case of some profiles indicate that for the latter no simple law could be established. These are the positions at which the secondary flows gave rise to particularly extreme velocity relations at the wall. The development of the secondary flow is especially responsible for the often irregular succession of the exponents in the various cross sections. In the case of the fully built-up velocity profile in section 0, it was possible to establish throughout the value $1/7$ for the exponent in agreement with the measurements of Nikuradse (reference 9). The measure of the accuracy and the region of validity of this $1/7$ power law are indicated in figure 29.

In concluding this section, there will also be given the drop in pressure head along the entry run, that is, in the z direction. For measuring this drop, three orifices are made at each section (b in fig. 8), one at the center of the bottom and two at the side walls of the rectangular pipe. The pressure readings of the three orifices gave very good agreement among themselves for each cross section. Pressure measurements at the interior of the cross sections were not taken, on account of the difficulty mentioned of applying the sphere apparatus. In figure 28 for an air velocity $c_{zm} = 16.3$ m/s, the change in the pressure head h in m of gas column is plotted against the entry length. The pressure head for the length of run 0 is obtained by computation. Assuming for this position that the mean velocity $c_{zm} = 16.3$ m/s extends over the entire cross section, there is found then, according to the Bernoulli law,

$$\frac{p}{\gamma_L} = - \frac{c_{zm}^2}{2g} = -13.6 \text{ m gas column}$$

As may be seen from figure 28, the value so obtained fits in very well with the pressure head curve, the latter being almost straight. Only for the first half of the entry run is there found a greater steepness in the curve and hence a somewhat larger pressure loss. This additional loss is due mainly to the fact that the mean velocity head

increases from the value $\left(\frac{c_z^2}{2g} \right)_m = 13.6$ m gas column at

in the initial section to the value 15.4 meters air column at section VI. From section VI to section 0, there is no further rise. The mean velocity head is determined from the following relation

$$\begin{aligned} \left(\frac{c_z^2}{2g} \right)_m &= \frac{1}{V} \int_0^F \frac{c_z^2}{2g} dv = \frac{1}{c_{zm} F} \int_0^F \frac{c_z^3}{2g} df = \\ &= \frac{4}{c_{zm} F} \iint \frac{c_z^3}{2g} dx dy \end{aligned}$$

where V and F have the meaning already indicated and

x is the distance from the midpoint of the velocity profile, measured along the horizontal lines, and y is the distance from the midpoint of the velocity profile measured along the vertical lines (fig. 17). The evaluation of this double integral was obtained graphically. The loss coefficient λ_{an} at the position of the entry run at which the turbulent velocity profile was fully established is obtained from the relation

$$\lambda_{an} = \frac{dh}{dz} \frac{1}{\frac{U}{4F} \frac{c_{zm}^2}{2g}}$$

and is found to have the value $\lambda_{an} = 0.0173$, dh/dz denoting the drop in pressure head in the z direction.

A further and more detailed investigation of the velocity and pressure relations in the entry run was dispensed with as this would have carried the work beyond the present limits.

VIII. THE MEASURED VELOCITY AND PRESSURE DISTRIBUTION IN THE TRANSITION PIECES

To present the test results in such a manner as to bring out the development of the velocity distribution in the individual cross sections of the transition pieces is found to be not a very simple problem. The profiles measured in the same measuring plane at the different cross sections have different base lengths as a result of the deformation. In order to be able to compare such profiles with one another the velocity ratio $c_z/c_{z_{max}}$ is usually plotted against the nondimensional value x/b , where x is the distance from the profile midpoint and b denotes half the profile width. By making this plot for the comparison profiles, it is then possible to say whether any initial profile for the case investigated becomes flatter or steeper. By this method Nikuradse and Dönch (references 1 and 2) plotted the profiles for convergent and divergent rectangular channels and compared them, thereby establishing the fact that velocity profiles of flows in divergent channels always become steeper toward the center

whereas, in converging channels, they become flatter than in the case of parallel flow, a phenomenon which may be expected also in such cases from a consideration of the Bernoulli law.

The assumption underlying this procedure is that the

expression $\int_b c_z dx$ for the profiles to be compared should have the same value, that is, that the discharge per second should be the same. This requirement is taken into account in the above-mentioned works of Nikuradse and Dönch insofar as their investigations were restricted to parts of the flow very close to the main axis of a rectangular section and so far removed from the boundary walls parallel to this axis that the flow built up there is practically plane and the quantity flowing through the region under consideration remains constant. This, however, is not true in the present case, since at all sections of the transition piece the flow is three-dimensional. For this reason, a direct comparison of the different profiles in a measuring plane is not possible. It is necessary rather to consider the velocity distribution over the entire cross section. The best indication of the velocity distribution and its variation by the cross-section deformation is therefore provided by the isotachs (c_z/c_{\max} or $c_z/c_{st} = \text{constant}$) at the various cross sections, as was already found to be the case in the discussion of the velocity distribution and its development in the initial rectangular run. This method also leads to the possibility of characterizing the velocity distribution in the manner shown by the curves in figures 61 and 62, where the method of presentation employed for plane flows is applied to three-dimensional flows. These curves will be discussed more in detail later.

Tables 4 and 5 give as examples the manner of evaluating from the results of the sphere measurements the three velocity components c_x , c_y , and c_z , for the cross section 5 in the transitions $C \longrightarrow R(I)$ and $C \longrightarrow R(II)$. Figures 30 and 31 give the plots of the c_x and c_y components. These curves show nothing surprising and their shape is at least qualitatively as expected from the result of the change in shape at the walls, provided, of course, no separation takes place. The particles flowing in the neighborhood of the principal axis are the least affected by the change in direction and therefore have the smallest

c_x and c_y components. The deflecting effect increases gradually toward the wall and attains its maximum there. Correspondingly, the c_x and c_y components increase with decreasing distance from the wall and drop to zero when very close to the wall since here the resulting velocity c must also be zero.

Figures 32 and 33 show the plots of the c_z components given in tables 4 and 5 for the various measuring planes and on the same figures are also indicated for completeness the velocities measured with the pitot tube in the neighborhood of the wall. From these it is possible to obtain directly the isotach diagram for these cross sections (figs. 36 and 43).

For all four transition pieces investigated, the maximum velocity at the axis of the transition piece remains constant and the isotachs for the cross sections are so drawn as to join points of equal value of c_z/c_{max} . For normal flow, the value of c_{max} is 16.4 m/s for the transition circle \longrightarrow rectangle and 19.5 m/s for the transition rectangle \longrightarrow circle. It is superfluous to indicate for all cross sections the velocity distribution in the same detail as that for section 5 of the transition C \longrightarrow R(I) and C \longrightarrow R(II). As already remarked, the c_x and c_y distributions show nothing unexpected so that the indication of their values for each cross section may be dispensed with. For the same reason, it is not necessary to give the measured c_x and c_y components for the transition R \longrightarrow C(I) and R \longrightarrow C(II). Only the development of the c_z distribution as a result of the transition is of interest and will therefore be described. In figures 34 to 38, 41, and 48 to 55, are given the isotachs for the two transition pieces and flow directions. The development of the velocity distribution in the exit runs may be seen in figures 39, 40, 46, and 47. With regard to the latter, it is to be observed that the rectangular cross section III is at a distance of 2.0 m from section 0 and section IV at a distance of 4.2 m. The circular cross sections 13 and 15 indicated in figures 46 and 47 are respectively at the distances 2.5 and 4.5 m from cross section 10.

In the case of built-up turbulent velocity distribution in the entry run, three effects may be expected to operate on the velocity distribution in the transition pieces:

1. The locally arising retardations and accelerations.
2. The change in the turbulence mechanism.
3. The change in the ratio of the area of cross section to the friction boundary of the section.

As may be seen, particularly from the isotach diagrams for the transition piece II, the local retardations and accelerations have a large effect. In both transition pieces these effects arise in the sections 9 and 1. In the latter sections the flow which possesses only axial components c_z must either undergo transition to a flow which possesses also c_x and c_y components or a flow with all three components must be converted into a purely axial one, depending on the direction of transition. To obtain a change in velocity pressure, differences are required as is known across the velocity direction. To understand the development of the isotach curves, it is therefore necessary to have the accurate pressure distribution at each cross section of the transition pieces. This distribution, as previously mentioned, was also measured with the sphere apparatus and is given on figures 56 to 60 for the transitions $C \rightarrow R(I)$ and $C \rightarrow R(II)$. The pressure distributions for the transitions $R \rightarrow C(I)$ and $R \rightarrow C(II)$ have fundamentally the same appearance, so that they need not be given. On these figures are shown the isobars, the numbers at each curve giving the reduced pressure heads in meters air column for a flow of air with mean velocity of $c_{zm} = 14.0$ m/s. In the case of transition piece I, different pressures at different points of the same section are found only for the sections 9 and 1 (figs. 56 and 57). For all other intermediate sections of transition piece I, no differences in pressure were found over the same section. From the discussion given below of the development of the isotach diagrams in transition piece I, it will be seen, however, that in the cross sections immediately preceding and following sections 9 and 1 near the walls there must be a small pressure rise or drop as an effect of the deflection of the flow. The aftereffects are stronger in the more steeply built transition piece II (fig. 59). As a result of the stronger deflections in the case of transition piece II, higher pressure differences arise over the cross section situated at the deflecting position, which still show up so strongly at section 5 that no unique constant pressure could be measured over the entire cross section. Cross sections 0 and 10 of transition piece II are again so far removed from the deflecting position that for these a distribution with con-

stant pressure could be obtained for both flow directions. Also, there should be observed, with regard to the pressure distributions, that they have the typical appearance to be expected. At each cross section at which there is a deflection, four pressure regions are built up along the wall, namely, two low and two high pressure regions as compared with the pressure at the center portions of the cross sections. These high and low pressures are of different magnitude, depending on the measuring plane in which they are considered, since deflections of varying magnitude occur in the different measuring planes. Thus, for example, in section 9 of the transition $C \rightarrow R(I)$ and $C \rightarrow R(II)$, the particles lying in the measuring planes 5, 6, and 7, must be more deviated than those in measuring planes 4 and 8. For this reason, the high pressures arising at the wall in measuring planes 5, 6, and 7, are greater than in 4 and 8. The same considerations can also be applied for the negative pressure arising at the side walls. In the interior of the cross section there are superimposed, according to the position of the point considered, the effects of the positive and negative pressures, so that a resultant pressure distribution is built up there.

IX. MORE DETAILED CONSIDERATION OF THE VELOCITY DISTRIBUTION

Figures 35 to 40, 42 to 47, 49, and 51, show first of all that the isotachs adjust themselves very rapidly to the new cross section contours. Particularly do the isotachs in the immediate neighborhood of the walls follow the contours of the cross sections closely, even at the corners, whereas those more at the center are naturally not so strongly affected. An exception is formed in the case of the isotachs in cross sections 1 and 9 for the transitions $C \rightarrow R(II)$ and $R \rightarrow C(II)$ (figs. 48, 50, 52, and 54). In the case of the latter cross sections the large pressure differences due to the strong flow deflections result in a completely different behavior. Thus, for example, in the transition $C \rightarrow R(II)$, the air in measuring planes 12, 13, or 14, flowing into section 9, meets a region with greatly lowered pressure and therefore the velocity head increases. Relatively high velocities arise therefore at the wall also, so that a very rapid velocity rise takes place from the wall to the interior of the section. The reverse is true for the air in the measuring planes 4, 5, 6, 7, etc., where, due to the deflection, there arises at section 9 a high pressure as compared with that at the center portions so that the air particles must give up kinetic energy in order to be pushed into the region of

higher pressure. This explains at least qualitatively the very slow rise of the velocity as shown by the isotachs. This phenomenon, according to which the velocity distribution in the case of accelerated flow becomes flatter and, in the case of retarded flow, sharper, is in full agreement with the test results already mentioned of Nikuradse and Dönch for plane flow.

Similarly, the irregular rise of the velocities at the wall is to be ascribed to local retardations or accelerations, as was found for cross sections 7, 5, and 3, of the transition $C \longrightarrow R(I)$ (figs. 35, 36, and 37) and in cross section 5 of the transition $C \longrightarrow R(II)$, depending upon whether the velocity distribution considered is in a horizontal or perpendicular measuring plane. As already remarked, the pressure does not immediately equalize after the deflection, so that also in the cross sections following the deflection cross section, accelerations and retardations occur. However, in cross section 5 of the transition $C \longrightarrow R(I)$, there already hardly appear pressure differences over the cross section. The isotach diagram nevertheless shows also for this cross section that at the side walls the velocity drop is smaller than at the bottom wall while it would be expected that the conversion of the kinetic energy into pressure energy and conversely ends there so that at all positions of the cross section there is the same velocity rise at the wall. This apparent contradiction finds its explanation in the consideration of the losses occurring during the energy conversions. It is generally known that a retardation of a medium along a friction wall leads to large pressure losses while acceleration leads to only small losses. Now such retardations along the wall occur in the measuring planes 12, 13, 14, etc., in the cross sections immediately following section 9 so that the flowing particles there lose velocity not only as a result of the conversion of kinetic to pressure energy but also through the friction of the wall and there thus arises an additional velocity loss. These effects may naturally still be observed in section 5. They can only disappear if new energy can be transported from the "healthy" flow in the interior of the sections to the particles at the wall. This transport of kinetic energy can only take place through the turbulent exchange. This is confirmed by consideration of the isotach diagrams for the transition $R \longrightarrow C(I)$. It is found that, for example, in cross section 5 there are no effects in the velocity distribution as a result of retardations along the wall but that the velocity rise in the neighborhood of the wall is the

same along the entire circumference although also for this transition retardations occur along the wall in the cross sections ahead of cross section 5. This different behavior is explained by the fact that through the existence of the secondary flow the turbulence is so strong that the slowed-up particles at the wall can always be supplied with new kinetic energy. That the fluctuating turbulent velocities in the transition rectangle \longrightarrow circle are greater than for the reverse transition must also be concluded from the much stronger fluctuations to which the fluid columns of the micro manometers used for measuring the velocity were subjected.

From the isotach curves for the transitions $R \longrightarrow C(I)$ and $R \longrightarrow C(II)$ it may also be clearly made out that the secondary flows are gradually destroyed on receding from the walls and a new turbulence mechanism comes into play. The effects of the secondary flows on the isotachs do not vanish completely, however, until after the flow has passed through a considerable length of pipe. Thus it may be seen that even after a circular exit run of 4.5 m the isotachs in the center portions of cross section 15 still show the characteristic indentations of the secondary flows. From this it may be concluded that the velocity distributions in the intermediate cross sections of a transition piece for regions not directly close to the wall depend essentially on the velocity distribution at the entrance. Since the velocity distribution at the end cross section is produced by the turbulence mechanism acting there, the result may also be expressed by saying that the change in the entire turbulence mechanism associated with the change in the cross-section shape hardly affects the velocity distribution in the transition piece itself. This is also understandable for the case of our relatively short transition lengths since it is known that the turbulent mechanism for example in the flow through a circular pipe must act on an initial length of run of about 90 diameters in order to produce a built-up velocity distribution.

In the present state of turbulence investigation for three dimensional flows it is unfortunately not yet possible to give more accurate numerical data on the changed turbulence mechanism produced by the transition piece which data would consist of the accurate mixing length distribution and its variation for each cross section. For this computation it would be necessary to extend the shear stress

law $\tau = \rho l^2 \left(\frac{dc_z}{d\eta} \right)^2$ mentioned in section VI for the two-dimensional case to three-dimensional flows (references

7, p. 325, and 8). The law thus extended has not yet been tested even for fully built-up three-dimensional turbulent flow as would be necessary before application is made to varying velocity distributions such as those in the transition pieces. Even if it were succeeded in computing the mixing length distribution according to the extended shear stress law the true turbulence mechanism would not yet be described since through the occurrence or vanishing of secondary flows further forces arising from the oscillation of the particles in the direction of the isotachs would be effective by acting on the flow which forces are not taken into account by the shear stress law and for which quantitative information is still impossible to obtain. It is therefore evident why the attempt to give a numerical account of the turbulence mechanism and its variation due to the transition will be dispensed with here.

For a further characterization there was therefore employed the method already applied for two-dimensional flow, namely, that of determining the exponents for the velocity distribution (c_z components) in the neighborhood of the wall of the various sections for the various measuring planes. These exponents were found in the same manner as for the rectangular entry runs. The values of the denominator n are collected in tables 6 and 7 for the two transition pieces investigated and for each direction. As may be seen, for all profiles whose measuring planes were sufficiently far removed from the parallel walls so that there was a unique distance from the wall an exponent could be determined at least for the layers next to the wall. No separations from the wall were found for any transition. From table 6 for the transition $C \rightarrow R(I)$ it may be seen that wherever local retardations occur the exponent $1/n$ is greater than at the initial profile whereas for local accelerations it remains the same or becomes somewhat smaller. This fact is even more evident from a consideration of table 6 for the transition $C \rightarrow R(II)$ where for accelerations values such as $1/21.0$ occur for the exponents and for retardations values such as $1/2.6$ while in the initial profile the value $1/8.3$ holds over the entire profile. This phenomenon is to some extent in contradiction with the measurements of Nikuradse. The latter finds in his tests on convergent and divergent channels of small opening angle that the $1/7$ power law obtaining at the initial section is not changed by retardation or acceleration. Besides the fact that the results of the two works are not directly comparable in this re-

spect since in Nikuradse's case there was retardation or acceleration over the entire cross section whereas in our case only local retardations or accelerations with constant pressure occur over a cross section this difference may perhaps be explained by table 7 in which the exponents are given for the transition $R \rightarrow C(I)$. There it will be found that the exponents in the accelerated or retarded portions at least for the portions of the wall lying in the neighborhood of the major and minor axes of the cross section are not different but equal to that at the initial profile. This different behavior as compared with the transition $C \rightarrow R(I)$ is again to be ascribed to the secondary flows. Since Nikuradse, as already remarked, investigated only the velocity distributions in a middle plane of the rectangular channel and the angles of divergence were of the same order of magnitude as those of transition piece I it is possible that the secondary flows occurring in his case and hence the increased turbulence similarly led to the result that for all cross sections in the middle plane of the convergent or divergent channel the $1/7$ power exponential law was found to hold.

In concluding this section there will be considered the effect of the change in magnitude of the friction areas due to the change in shape of the cross section on the velocity distribution. Figures 61 and 62 show curves which were obtained from the isotach diagrams the values of c_z/c_{max} being plotted against the ratio expressed in percent of the area enclosed by an isotach to the entire cross section area, the areas being obtained by planimeter. Comparison of two such curves at different cross sections is sufficient to show in general whether the velocity distribution over the entire cross section becomes fuller or more tapered as a result of the deformation. For the transitions $C \rightarrow R(I)$ and $C \rightarrow R(II)$ it may be seen from figure 61 that the velocity distribution becomes as was expected more tapered in cross section O. Similarly the flattening of the velocity distribution through the transition $R \rightarrow C(II)$ (fig. 62) quite corresponds to the expectation. On the other hand it is surprising that for the transition $R \rightarrow C(I)$ the velocity distribution becomes more tapered, since in this case it would also be assumed that as a result of the decrease in the frictional circumference the proportion of particles with relatively small velocities would become smaller and there would thus occur a flattening of the velocity distribution. If account is taken of the fact, however, that the changed velocity distribution due to the

cross section deformation depends not only on the change in magnitude of the friction areas but also on the previously mentioned two effects, namely, the local retardations and accelerations and the turbulence mechanism, which play an important part then the curves of figures 61 and 62 may be explained in the following manner: As already said, for all four transitions in the cross sections 0 and 10 no pressure differences were found in the cross section plane. There is thus available for each air particle the same amount of pressure energy for its path through the corresponding transition piece. The particles with small velocity near the wall lose still more kinetic energy while those more toward the center with relatively larger velocities are entirely unaffected or only slightly affected by these local retardations and so flow with considerably smaller pressure loss so that they are even accelerated somewhat by the excess pressure energy. If in addition there is an increase in the frictional perimeter of the cross section during the transition the two effects are superposed in the same sense so that for such cases the plotted velocity distribution becomes more tapered (fig. 61). For the converse case, that is, where the friction surface is reduced as a result of the cross section deformation no such general statement can be made for the velocity distribution since it is a question as to which of these two effects is preponderant. From figure 62 it must therefore be concluded that for the transition $R \longrightarrow C(I)$ the effect of the arising local retardations is preponderant over that of the decrease in the perimeter of the cross section while for the transition $R \longrightarrow C(II)$ the reverse is true. The reason for this different behavior may perhaps be sought in the fact that the secondary flow due to the short transition length of piece II is still so strong even after the transition that the particles stopped at the wall can immediately receive new kinetic energy by the turbulence interchange while as a result of the larger transition length of piece I the secondary flows are gradually destroyed already at the walls of the transition piece so that this turbulence interchange cannot take place to the same extent as for the transition $R \longrightarrow C(II)$. Considering figures 61 and 62 in the light of this view it may be said that only for transition $R \longrightarrow C(II)$ is there any directly evident effect of the magnitude of the cross section friction perimeter.

X. THE PRESSURE DROP IN THE TRANSITION PIECES

On figures 63 and 64 there is plotted for all four investigated cases the drop in pressure at the wall in meters air column against the pipe length for a portion of the entry run, the transition piece and the exit run. The difference in the initial pressure of cross section 10 for the transitions $C \rightarrow R(I)$ and $C \rightarrow R(II)$ is to be ascribed to the fact that in the transition $C \rightarrow R(II)$ the entry run was somewhat shorter than for transition $C \rightarrow R(I)$. The measured wall pressures for the sections 9 and 1 of the transition pieces which pressures are different depending on whether the side or bottom orifices are used for the measurement are omitted. The variation of the wall pressure along an axial section of the transition piece naturally provides no measure for the losses occurring if the pressure in the interior of the cross section is not constant and does not agree with that at the wall. The typical appearance of these curves is for all cases the same. As a result of the conversions occurring in the transition pieces of kinetic into pressure energy and conversely the pressure in the first portion of the transition piece rises more strongly than in the entry run and again sinks toward the end of the transition. These energy conversions come to an end only when the pressure in the exit run is again linear. For all transitions this condition obtains after a final length of run of $l_a' = 0.5$ m. Considering the pressure difference between the inlet and outlet flange of the transition piece without taking account of the partial pressure gain in the exit run as pressure head loss h_v of the transition piece of total length l_v there is obtained by substituting the mean hydraulic diameter of

$$d_{hv} = 4 \frac{F}{U} = 4 \frac{F_C + F_R}{U_C + U_R} = 0.173 \text{ m}$$

into the loss equation

$$h_v = \lambda_v \frac{l_v}{d_{hv}} \frac{c_{zn}^2}{2g}$$

the values given in table 8 for the loss coefficient.

There are also given in this table values for a λ_a' that was determined for the 0.5 m piece l_a' of the exit run in which further energy conversions take place. On comparing the values of λ_v and λ_a' it will be seen that these values come out considerably smaller for the transitions $R \longleftrightarrow C(I)$ and $R \longrightarrow C(II)$ than for the transitions $C \longrightarrow R(I)$ and $C \longrightarrow R(II)$. The reason for this difference must be the increase in the mean velocity head $c_{zm}^2/2g$ in the transitions $C \longrightarrow R(I)$ and $C \longrightarrow R(II)$ which in the case of the transitions $R \longrightarrow C(I)$ and $R \longrightarrow C(II)$ remains practically constant. The mean velocity head in the different cross sections was determined by the method already mentioned in the consideration of the pressure variation along the rectangular entry run. For the transitions $C \longrightarrow R(I)$ and $C \longrightarrow R(II)$ there was obtained an increment in the mean velocity head from 10.3 m in cross section 10 to 11.45 m in cross section 0.

If it is desired to find which of the two transition pieces is better with regard to the pressure losses we should not restrict ourselves naturally to the comparison of the values of λ_v and λ_a' but must compare the sums formed of the products $\lambda_v \frac{l_v}{dh_v} \frac{c_{zm}^2}{2g}$ and $\lambda_a' \frac{l_a'}{dh_a} \frac{c_{zm}^2}{2g}$.

If this comparison is carried through for the transitions $C \longrightarrow R(I)$ and $C \longrightarrow R(II)$ it will be found that the transition piece II causes a smaller pressure loss and so is better suited for the transition circle \longrightarrow rectangle. For the direction of transition rectangle \longrightarrow circle the result is arrived at that both transition pieces are equivalent. This at first rather surprising result becomes explainable on considering figure 55 from which it may be seen that for cross section 10 in the transition $R \longrightarrow C(II)$ the still very strong secondary flow in the immediate neighborhood of the wall in section 10 of transition $R \longrightarrow C(II)$ leads to very large velocity drops which naturally result in increased losses and bring about the result that the transition piece II in spite of its smaller length produces the same pressure drop as transition piece I.

It must still be pointed out that these findings with regard to the relative efficiency of the transition pieces are justified only in the case where there exists a built-up turbulent velocity distribution at the entrance to the

transition piece. If other velocity distributions exist the question of the relative efficiency of the transition pieces may be differently decided since different velocity distributions result in different energy distributions and the latter are of very great effect on the pressure loss.

In conclusion attention is called to the loss coefficients λ_{an} and λ_a in table 8. These coefficients correspond to those parts of the entry and exit runs in which there is a linear relation between pressure loss and pipe length. The two columns agree very well and this moreover brings out the justification for the customary introduction of the hydraulic diameter for the determination of the pressure loss of pipes of noncircular cross section.

XI. SUMMARY

In this paper the results are presented of pressure and velocity distribution measurements in transition pieces in order to investigate the effect of the change in shape of the cross section contour for equal area of cross section. For the two investigated transition pieces which differed in their transition lengths a circular cross section is deformed into one of rectangular perimeter. Since in each transition piece measurements were taken for flows in each direction four different cases were considered. The entry runs connected ahead of the transition pieces were chosen of such length as to obtain a built-up turbulent velocity distribution at the end of the run. For this purpose velocity measurements in the entry run of the rectangular pipe were necessary. For circular pipe section these velocity distributions are sufficiently well known.

The velocity distributions measured in the various deformed cross sections are brought out by means of isotach diagrams. The isotachs at each cross section very rapidly assume the shape of the corresponding cross section provided the local retardations and accelerations do not become too large. There is shown the existence of an exponential law for the velocity in the neighborhood of the wall in each of the measuring planes parallel to the axis.

The most important factors affecting the velocity and pressure distribution in the transition pieces are named

and it is attempted to show their effects at least qualitatively. The greatest effect is that produced by the local retardations and accelerations. It is particularly difficult to determine the effect of the change in the turbulence mechanism through the cross section deformation on the velocity distribution. Since in a rectangular pipe the turbulence of the flow shows up directly by the presence of secondary flows it is concluded from the measurements for the transition rectangle \longrightarrow circle that the change in the turbulence mechanism due to the cross section deformation does not very greatly affect the velocity distribution in the transition cross sections themselves. A third effect indicated is the change in the friction perimeter of the cross section due to the deformation. The establishment of this effect is also rendered difficult by the fact that there is no method for finding this effect independently of the other two. An important fact established is that in no transition piece did separation from the wall occur.

At the conclusion of the paper are given the loss coefficients for the two transition pieces in both flow directions.

Translation by S. Reiss,
National Advisory Committee
for Aeronautics.

REFERENCES

1. Nikuradse, J.: Untersuchungen über die Strömungen des Wassers in konvergenten und divergenten Kanälen. VDI-Forschungsheft 289, Berlin, 1929.
2. Dönch, F.: Untersuchungen über divergente und konvergente turbulente Strömungen mit kleinen Öffnungswinkeln, VDI-Forschungsheft 282, Berlin, 1926.
3. Nippert, H.: Über den Strömungsverlust in gekrümmten Kanälen, VDI-Forschungsheft 320, Berlin, 1929.
4. Schröder, E. Strömungsuntersuchungen an einem Rotationshohlraum, Mitt. Inst. Strömungsmaschinen T. H. Karlsruhe H. 2 (Hrsg. W. Spannhake), Berlin: VDI-Verlag 1932.
5. Kirsten, H.: Experimentelle Untersuchung der Entwicklung der Geschwindigkeitsverteilung bei der turbulenten Rohrströmung. Diss. Univ. Leipzig 1927.
6. Krisan, F.: Speed and Pressure Recording in Three-Dimensional Flow. T.M. No. 688, N.A.C.A., 1932.
7. Wien and Harms: Handbuch der Experimental-Physik, vol. 4, pt. 1, p. 505. Leipzig: Akadem. Verlagsges. 1931.
8. Prandtl, L.: Turbulent Flow. T.M. No. 435, N.A.C.A., 1927.
9. Nikuradse, J.: Untersuchung über die Geschwindigkeitsverteilung in turbulenten Strömungen. VDI-Forschungsheft 281, Berlin, 1926.

Table I
Cross section areas
for piece I

No. of section	Area cm ²
10	288,6
9	288,6
8	284,6
7	283,6
6	282,2
5	282,5
4	281,5
3	281,4
2	281,0
1	285,5
0	284,5

Table III
Value of n for various positions of
entry run

Meas- ur- ing plane	Cross section								
	I	II	III	IV	V	VI	VII	VIII	0
12	8,1	6,0	6,0	8,4	6,0	8,5	11,0	8,3	7,0
13	9,0	5,2	6,5	7,4	6,0	8,3	7,5	8,3	7,0
14	6,5	6,0	6,5	5,5	—	7,3	7,4	7,2	7,0
14a	7,0	6,5	6,5	6,5	—	7,3	8,0	8,3	7,0
14b	5,0	6,0	6,8	6,3	—	7,0	9,0	8,0	7,0
14c	5,0	5,2	7,0	6,6	—	6,5	10,4	8,0	7,0
6	8,0	5,5	12,5	7,2	8,4	13,5	9,0	8,3	7,0
7	8,0	6,0	12,5	6,5	9,5	11,1	9,3	8,5	7,0
8	8,0	6,2	9,7	6,7	8,4	10,1	9,4	7,9	7,0
9	14,0	6,0	8,7	6,7	11,0	9,3	8,3	7,8	7,0
10	8,5	6,6	9,2	6,7	11,0	8,2	8,0	7,0	7,0
11	6,5	—	8,8	6,3	—	8,4	6,3	6,6	7,0
11a	7,0	—	8,5	6,7	—	7,6	5,9	5,3	7,0
11b	8,0	—	8,3	7,7	13,6	6,5	5,4	5,6	7,0

Table II
Cross section areas
for piece II

No. of section	Area cm ²
10	288,6
9	288,6
5	281,0
1	282,4
0	287,6

Table VIII
The loss coefficient λ .

Transi- tion	λ_{an} Entry run	λ_v Transi- tion	$\lambda_{a'}$ Exit run	λ_n Exit run
C \rightarrow R (I)	0,0162	0,0248	0,0266	0,01665
C \rightarrow R (II)	0,0162	0,0237 ✓	0,0228	0,01665
R \rightarrow C (I)	0,0173	0,0106	0,0117	0,0171
R \rightarrow C (II)	0,0173	0,0199 ✓	0,00934	0,0171

Table IV
Evaluation of sphere measurements at section 5 of transition C \rightarrow R(I)

Measuring * y point x		α Deg.	δ Deg.	ψ Deg.	c m/s	c_x m/s	c_y m/s	c_z m/s	p/γ_L m GS
12	6	0	0	0	16,38	0	0	16,38	-41,6
12	7	+ 0,8	0	+ 11,7	16,38	+ 0,223	- 0,046	16,37	-41,5
12	8	+ 1,5	- 1	+ 22,2	16,4	+ 0,50	+ 0,101	16,20	-41,6
12	9	+ 2	- 2,5	+ 31,6	15,92	+ 0,835	+ 0,298	15,38	-41,4
12	10	+ 2,5	- 4	+ 39,6	15,12	+ 1,185	+ 0,331	15,08	-41,5
12	11	+ 4,5	- 5,1	+ 44,8	12,05	+ 1,395	+ 0,055	11,95	-41,6
13	6	+ 0,5	+ 0,5	+ 0,1	16,35	+ 0,142	+ 0,143	16,32	-41,7
13	7	+ 2,5	+ 1,1	+ 9	16,35	+ 0,653	- 0,44	16,32	-41,6
13	8	+ 4	+ 0,6	+ 18,1	16,32	+ 1,02	- 0,533	16,30	-41,4
13	9	+ 5	0	+ 26,3	16,25	+ 1,265	- 0,627	16,20	-41,6
13	10	+ 5,5	- 1	+ 33,5	15,35	+ 1,371	- 0,577	15,27	-41,6
13	11	+ 4,5	+ 4,5	+ 39,5	11,94	+ 1,325	- 0,125	11,88	-41,7
14	6	+ 0,5	+ 1,2	+ 0,7	16,29	+ 0,137	- 0,375	16,21	-41,5
14	7	+ 3	+ 2	+ 7,5	16,15	+ 0,763	- 0,658	16,12	-41,6
14	8	+ 4,5	+ 1	+ 15,2	15,98	+ 1,132	- 0,598	15,9	-41,7
14	9	+ 6	0	+ 22,5	15,62	+ 1,42	- 0,588	15,55	-41,6
14	10	+ 6,5	+ 1,6	+ 29,3	14,76	+ 1,665	- 0,443	14,65	-41,7
15	6	+ 1,5	+ 1	+ 1,3	14,78	+ 0,398	- 0,247	14,72	-41,5
15	7	+ 4	+ 2	+ 6,4	14,72	+ 0,96	- 0,624	14,7	-41,5
15	8	+ 5,5	+ 1,5	+ 13,4	14,6	+ 1,277	- 0,696	14,5	-41,6
15	9	+ 8	+ 0,5	+ 20	13,4	+ 1,71	- 0,491	12,8	-41,6

* The measuring points are the intersections of the three planes.
1, Cross section 5. 2, Horizontal (x) plane. 3, Vertical (y) plane.

Table V
Evaluation of sphere measurements at section 5 of transition C \rightarrow R(II)

Measuring * y point x		α Deg.	δ Deg.	ψ Deg.	c m/s	c_x m/s	c_y m/s	c_z m/s	p/γ_L m GS
12	6	0	0	0	16,38	0	0	16,38	-36,6
12	7	+ 2	- 0,25	+ 10,8	16,38	+ 0,570	- 0,053	16,34	-37,0
12	8	+ 4	- 1,5	+ 20,8	16,28	+ 1,205	- 0,0018	16,20	-37,4
12	9	+ 6	- 3,3	+ 29,8	15,85	+ 1,88	- 0,0039	15,7	-37,75
12	10	+ 6,2	- 6	+ 37,5	14,85	+ 2,2	+ 0,274	14,65	-37,7
13	6	0	+ 2,5	0	16,38	0	- 0,712	16,38	-37,2
13	7	+ 2,5	+ 2,1	+ 9,0	16,37	+ 0,606	- 0,72	16,32	-37,0
13	8	+ 5	+ 1,9	+ 17,8	16,1	+ 1,175	- 0,918	16,02	-37,4
13	9	+ 7	+ 1,7	+ 25,6	15,78	+ 1,90	- 0,416	15,62	-38,0
13	10	+ 8,5	+ 5,3	+ 32,9	14,68	+ 2,54	- 0,0168	14,38	-37,8
14	6	+ 0,7	+ 6	+ 0,2	15,85	+ 0,178	- 1,66	15,72	-37,3
14	7	+ 4,5	+ 5,5	+ 8,2	15,8	+ 1,00	- 1,665	15,63	-37,3
14	8	+ 8	+ 4	+ 15,8	15,6	+ 1,785	- 1,635	15,4	-37,7
14	9	+ 11	- 0,2	+ 22,9	15,12	+ 2,667	- 1,077	14,82	-38,0
14	10	+ 13,5	- 5,7	+ 29,1	14,4	+ 3,62	- 0,387	13,92	-38,2
14	10b	+ 13,5	- 8,5	+ 32,1	13,45	+ 3,68	- 0,022	12,95	-38,3
15	6	+ 1	+ 11,25	+ 0,6	14,77	+ 0,228	+ 2,28	14,45	-37,5
15	7	+ 6,2	+ 11,2	+ 7,4	14,4	+ 1,122	- 2,293	13,90	-37,8
15	7	+ 13	+ 10	+ 14	13,58	+ 2,25	- 3,0	13,0	-38,2

* The measuring points are the intersections of the three planes
1, Cross section 5.. 2, Horizontal (x) plane. 3, Vertical (y) plane.

Table VI
Value of n at different sections of transitions $C \rightarrow R(I)$ and $C \rightarrow R(II)$

Measuring planes	Transition C→R (I)									Transition C→R (II)				
	Cross section									Cross section				
	10	9	7	5	3	1	0	III	IV	10	9	5	1	0
12	8,3	9,5	5,8	5,8	6,0	6,4	8,0	6,0	7,0	8,3	21	8,0	3,5	8,0
13	8,3	9,0	6,5	6,0	6,0	6,5	8,0	6,0	7,0	8,3	17	8,5	4,5	8,0
14	8,3	8,5	7,5	6,0	7,6	6,8	8,0	7,0	7,0	8,3	16	9,0	5,3	8,0
14b	8,3	8,0	8,0	8,0	8,0	8,0	8,0	8,0	7,0	8,3	14	10,0	8,8	4,5
6	8,3	7,2	8,0	8,0	8,0	8,5	8,0	7,0	6,8	8,3	2,6	7,4	21,5	8,0
7	8,3	7,5	8,0	8,0	8,0	8,5	8,0	7,0	6,4	8,3	3,0	8,0	18	8,0
8	8,3	7,5	8,0	8,0	8,0	8,0	8,0	7,0	6,5	8,3	6,5	8,0	13	8,0
9	8,3	7,7	8,0	8,0	8,0	7,6	8,0	7,3	7,0	8,3	8,0	8,0	7,6	8,0
9b	8,3	8,0	8,0	8,0	8,0	7,4	8,0	7,3	7,0	8,3	9,5	4,5	8,0	7,5
10	8,3	8,0	8,0	8,0	8,0	7,0	8,0	7,0	+	8,3	13,0	4,0	8,0	7,0
10b	—	—	—	8,0	8,5	6,8	8,0	7,3	+	—	—	3,9	6,5	6,0
11	—	—	—	—	11,0	6,7	9,0	7,5	+	—	—	—	4,0	5,6
11a	—	—	—	—	—	6,5	9,2	7,5	+	—	—	—	4,0	5,5

+ Signifies that for these measuring planes no exponential law could be established since the secondary flows give rise to extreme velocity distributions near the wall.

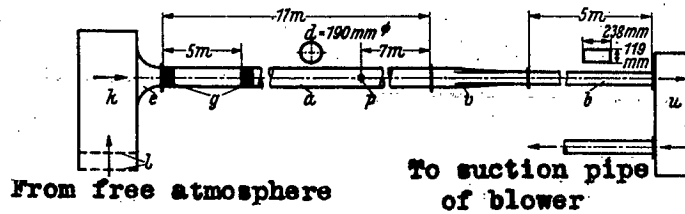
— Signifies that the corresponding measuring plane lies outside the cross section.

Table VII
Value of n at different sections of transitions $R \rightarrow C(I)$ and $R \rightarrow C(II)$

Measuring planes	Transition $R \rightarrow C(I)$									Transition $R \rightarrow C(II)$				
	Cross section									Cross section				
	0	1	3	5	7	9	10	15	0	1	5	9	10	
12	7,0	7,0	7,0	7,0	7,0	7,0	6,4	6,4	7,0	5,0	16,0	20,0	7,0	
13	7,0	7,0	7,0	7,0	7,0	7,0	6,2	7,1	7,0	5,5	16,0	20,0	12,0	
14	7,0	6,7	7,2	7,1	7,2	7,5	6,0	6,9	7,0	4,5	17,0	20,0	12,0	
14b	7,0	6,8	7,2	7,0	7,2	7,2	6,3	6,3	7,0	5,0	+	14,0	12,0	
6	7,0	7,0	7,0	7,0	7,0	7,0	7,0	6,8	7,0	21	5,5	5,7	6,7	
7	7,0	7,0	7,0	7,0	7,0	7,0	6,7	6,8	7,0	20	6,8	5,7	7,5	
8	7,0	7,3	7,0	7,0	6,7	6,5	6,5	7,3	7,0	13,4	7,0	5,6	7,0	
9	7,0	7,2	7,2	7,0	6,3	6,2	6,2	7,0	7,0	10,0	6,8	5,2	7,3	
9b	7,0	7,0	7,2	7,0	6,9	6,3	6,0	6,7	7,0	9,0	3,8	4,7	9,7	
10	7,0	7,0	7,2	6,9	7,8	7,0	6,5	7,4	7,0	7,5	3,5	12,0	8,3	
10b	7,0	7,0	7,6	7,0	—	—	—	—	7,0	7,5	2,0	—	—	
11	7,0	7,0	6,8	—	—	—	—	—	7,0	7,3	2,0	—	—	
11a	7,0	7,0	—	—	—	—	—	—	7,0	7,0	—	—	—	

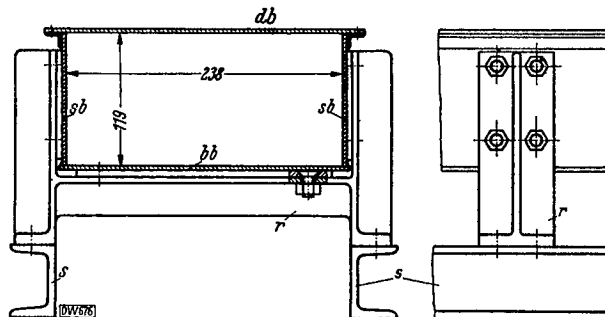
+ Signifies that for these measuring planes no exponential law could be established since the secondary flows give rise to extreme velocity distributions near the wall.

— Signifies that the corresponding measuring plane lies outside the cross section.



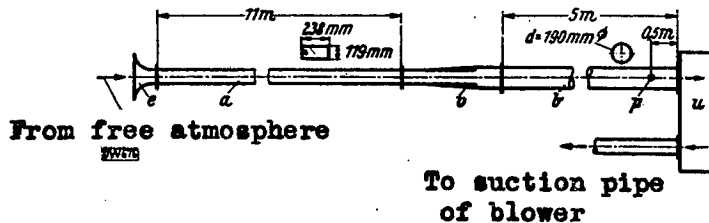
- | | |
|--|-----------------------|
| a, Entry run of circular section | k, Suction chamber |
| b, Exit run of rectangular cross section | l, Perforated sheet |
| d, Diameter of circular pipe | p, Prandtl tube |
| e, Inlet throat | u, Deflecting chamber |
| g, Honeycomb | v, Transition piece |

Figure 1.- Test set-up for the deformation of a circular into a rectangular cross section.



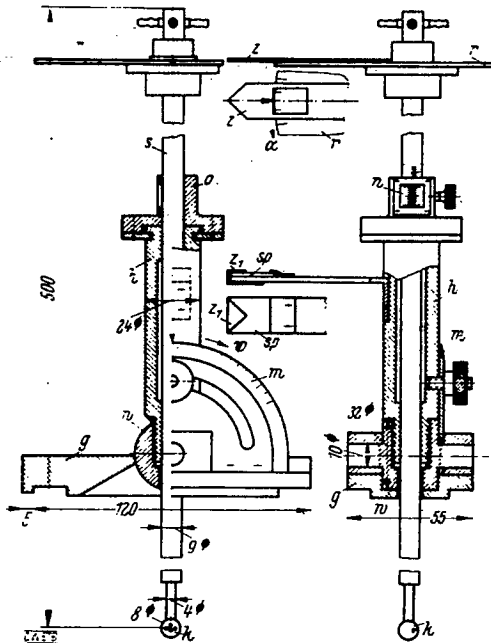
- | | | |
|-----------|------------------|-----------------|
| r, Frame | bb, Bottom sheet | db, Cover plate |
| s, U-beam | sb, Side sheets | |

Figure 2.- Cross section through rectangular channel.



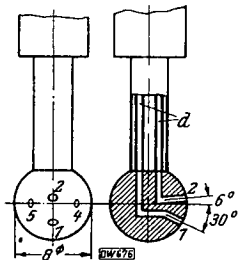
- | | |
|---|-----------------------|
| a, Entry run of rectangular cross section | e, Inlet throat |
| b, Exit run of circular cross section | p, Prandtl tube |
| d, Diameter of circular pipe | u, Deflection chamber |
| | v, Transition piece |

Figure 3.- Test set-up for the deformation of the rectangular into a circular cross section.



- g, Base plate
- h, Support
- k, Sphere
- m, Graduated circle for ψ
- n, Vernier
- o, Head piece
- r, Graduated disk
- s, Shaft of sphere
- w, Cylinder
- z, z_1 indicators
- sp, Mirror

Figure 4.- Pressure sphere apparatus.



d, Pressure tubes;
1 to 5 orifices

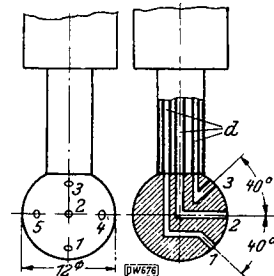
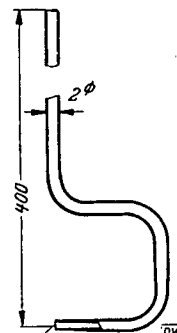


Figure 5a.- Pressure sphere employed
of 8mm diameter with
four orifices.

Figure 5b.- Pressure sphere of 12
mm diameter with five
orifices as previously employed.

Figure 7.- Pitot tube.



Inside diameter = 0.5 mm

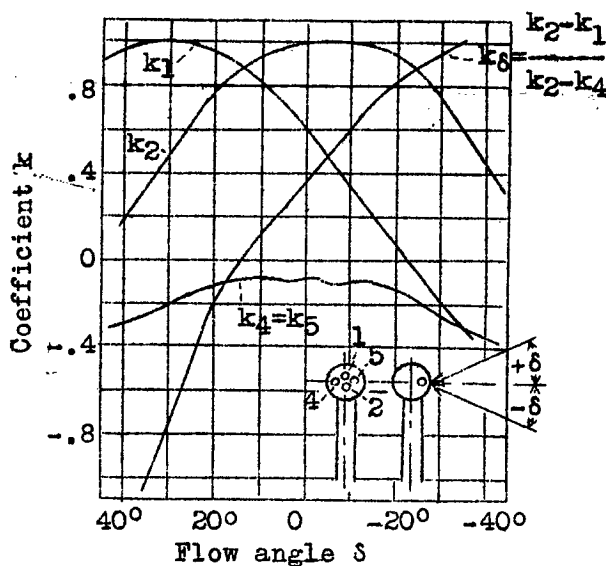


Figure 6.- Calibration curve of the pressure sphere employed with four orifices (see fig. 5a).

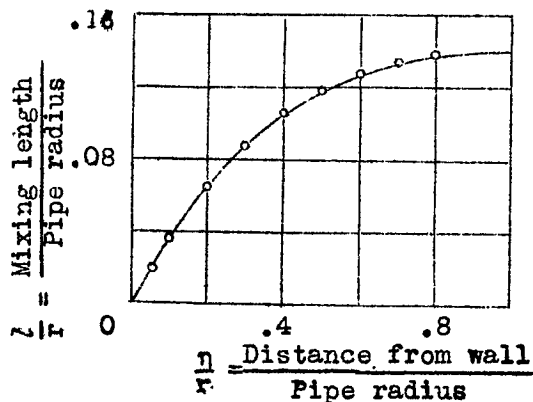


Figure 14.- Mixing length distribution as a function of the distance from the wall for cross section 10 of the transitions $C \rightarrow R(I)$ and $C \rightarrow R(II)$.

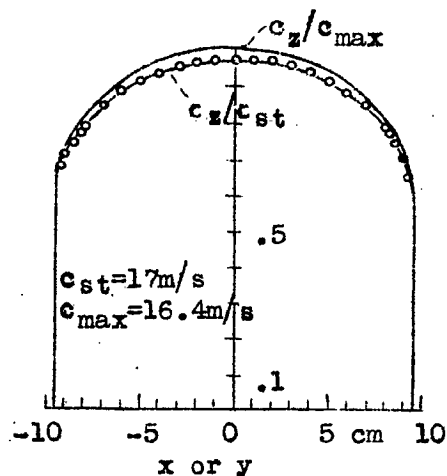


Figure 13.- Initial velocity profile in circular cross section 10 in the transitions $C \rightarrow R(I)$ and $C \rightarrow R(II)$.

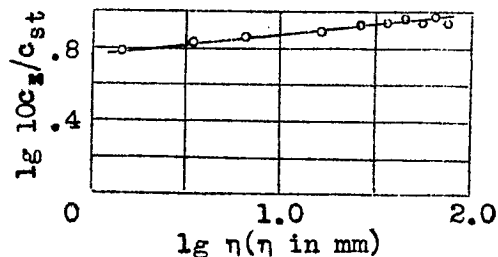
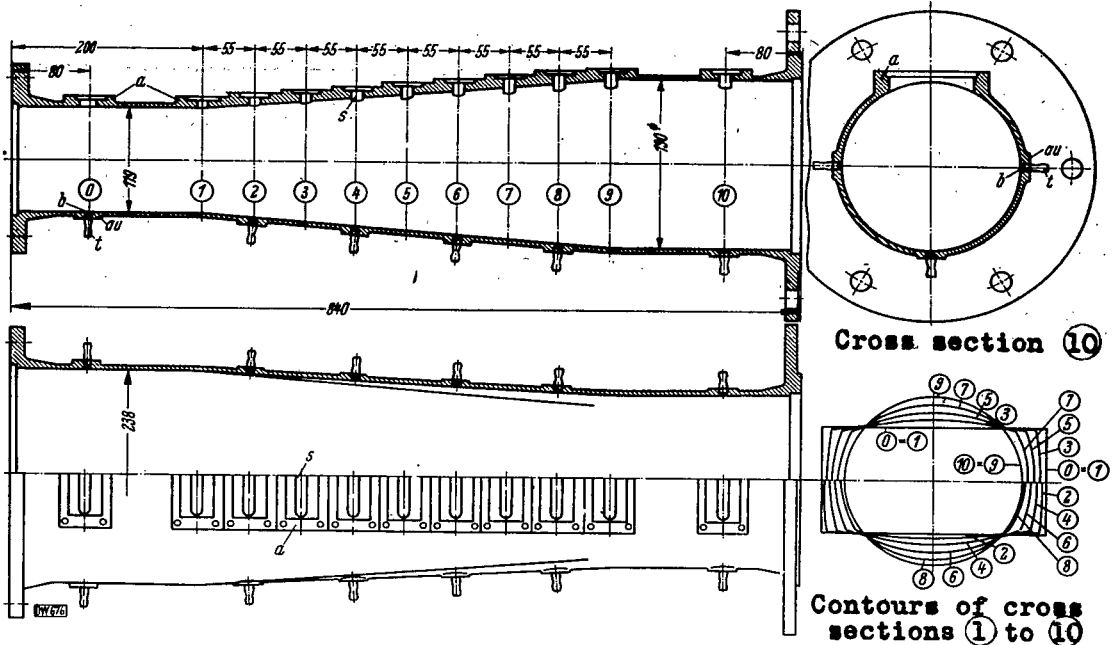


Figure 15.- Determination of the exponent $1/n$ for the velocity distribution in cross section 10 of the transitions $C \rightarrow R(I)$ and $C \rightarrow R(II)$.



a, Seats for screwing on the velocity measuring apparatus
s, Slots in a, leading into the interior of the pipe
au, b, t, Arrangement for attachment of a manometer

Figure 8.- Transition piece I.

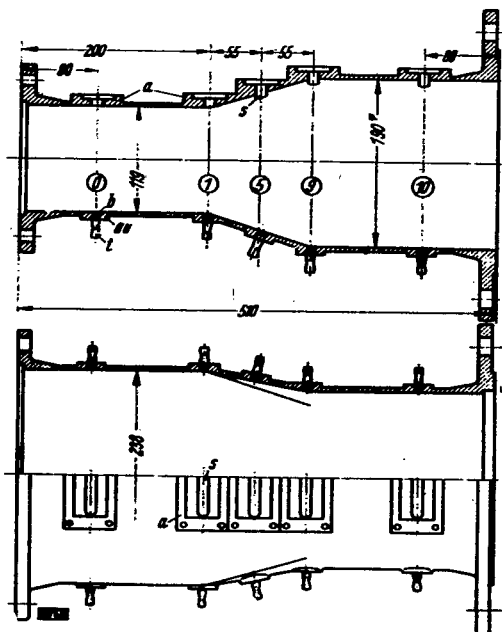


Figure 9.- Transition piece II.

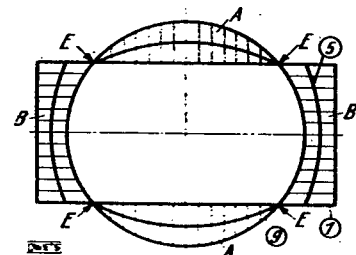
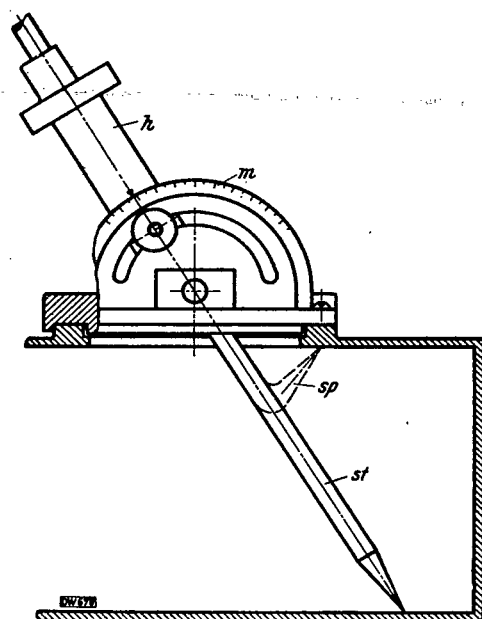


Figure 10.- Determination of the transition cross sections.



st, sp, Caliper points
h, Support
m, Graduated circle
(see also fig. 4)

Figure 11.- Caliper apparatus for measuring the transition cross section.

Figure 12.- Arrangement of measuring points in sections 10 and 0

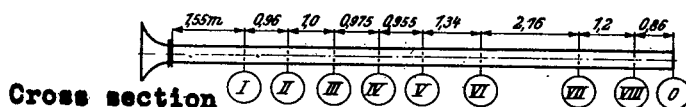
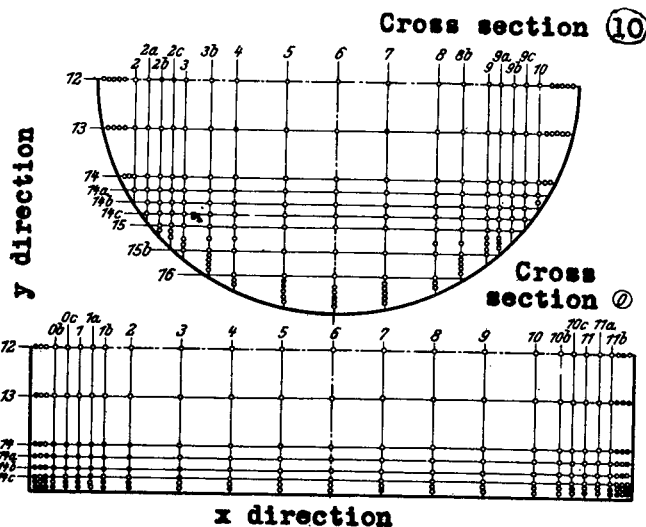


Figure 16.- Position of cross sections I to VIII and 0 in the rectangular entry run.

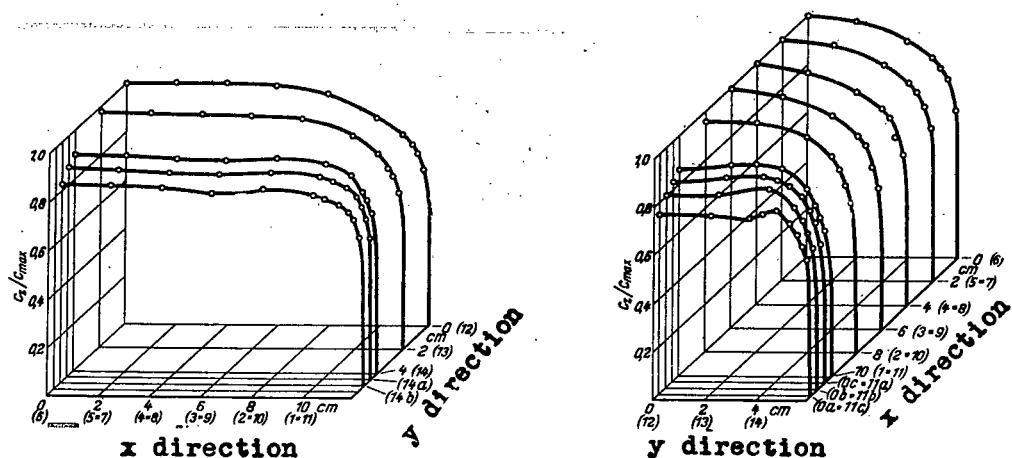
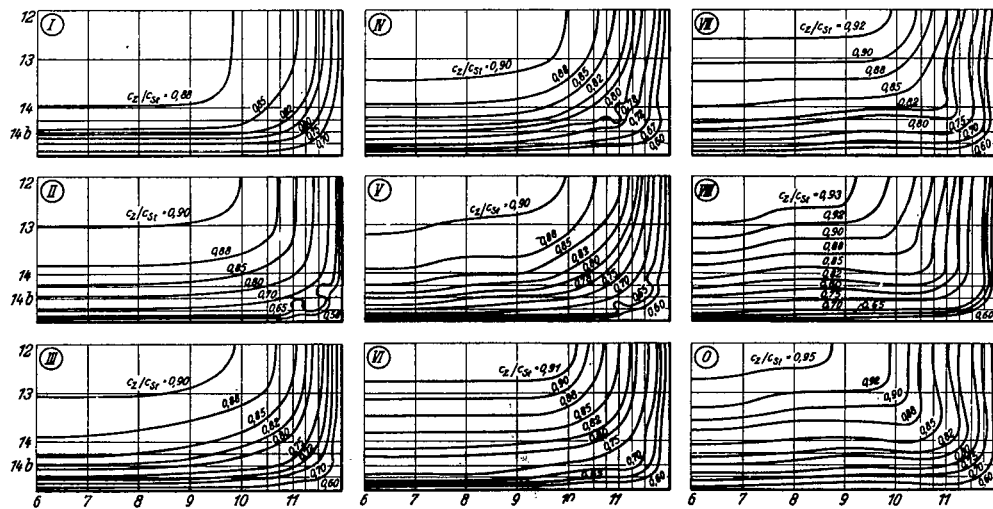


Figure 17.- Velocity distribution (c_z/c_{max}) in the horizontal (x) and vertical (y) measuring planes in cross section 0 of the transitions $R \rightarrow C(I)$ and $R \rightarrow C(II)$. $c_{max} = 19.5$ m/s (for the figures in parentheses see fig. 12).



Figures 18-25.- Isotachs in cross sections I to VIII of the rectangular entry run.

Figure 26.- Isotachs in cross section 0 of the transitions $R \rightarrow C(I)$ and $R \rightarrow C(II)$.

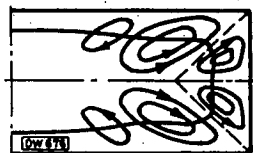


Figure 27.- Secondary flow in a pipe of rectangular section.

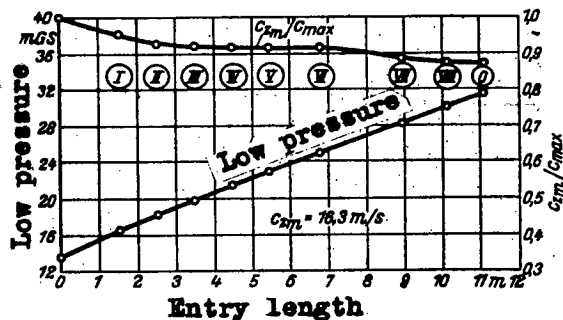


Figure 28.- c_{sm}/c_{max} and static pressure as a function of the entry length of the rectangular pipe.

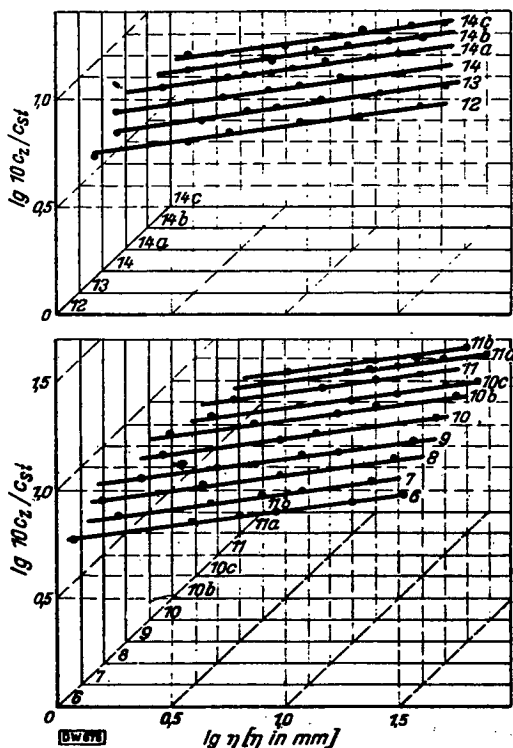


Figure 29.- Determination of the exponent $1/n$ of the velocity distribution in the neighborhood of the wall in the horizontal and vertical measuring planes of cross section O for the transitions $R \rightarrow C(I)$ and $R \rightarrow C(II)$.

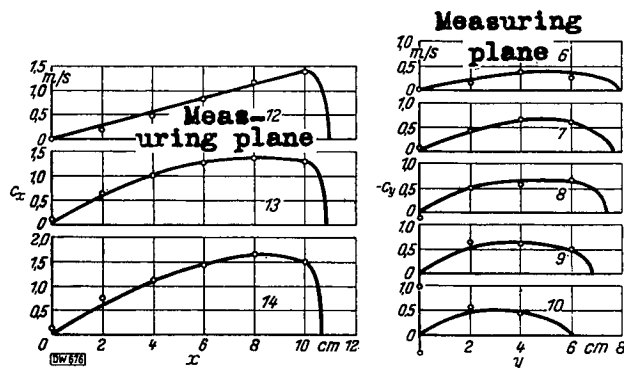


Figure 30.- c_x and c_y distributions in the horizontal and vertical planes respectively in cross section 5 of the transition $C \rightarrow R(I)$.

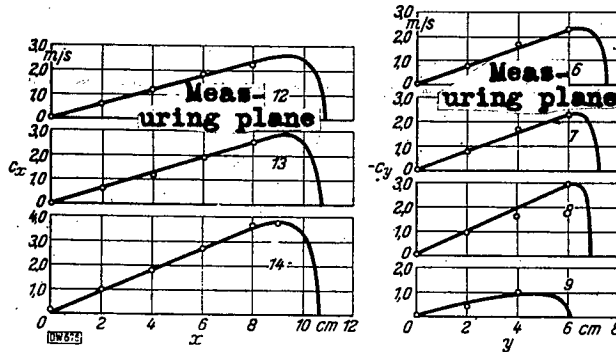


Figure 31.- c_x and c_y distributions in the horizontal and vertical measuring planes respectively for cross section 5 of the transition $C \rightarrow R(II)$.

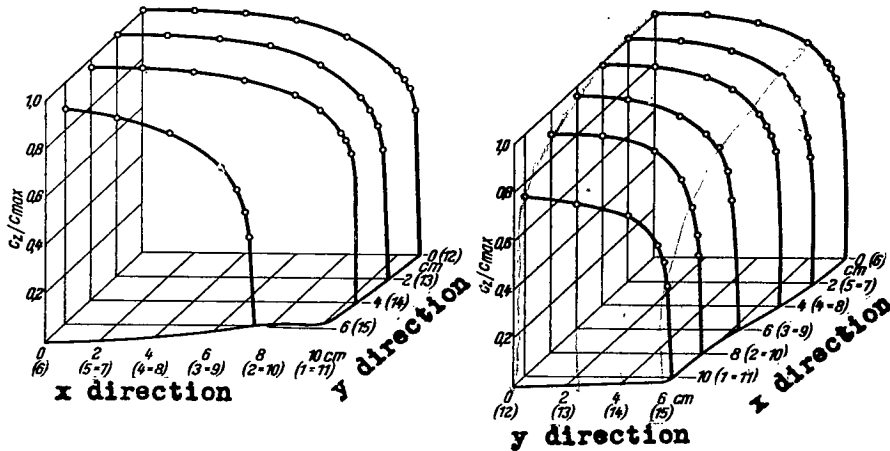


Figure 32.- Velocity distribution (c_x/c_{max}) in the horizontal (x) and vertical (y) measuring planes of cross section 5 of the transition $C \rightarrow R(I)$.

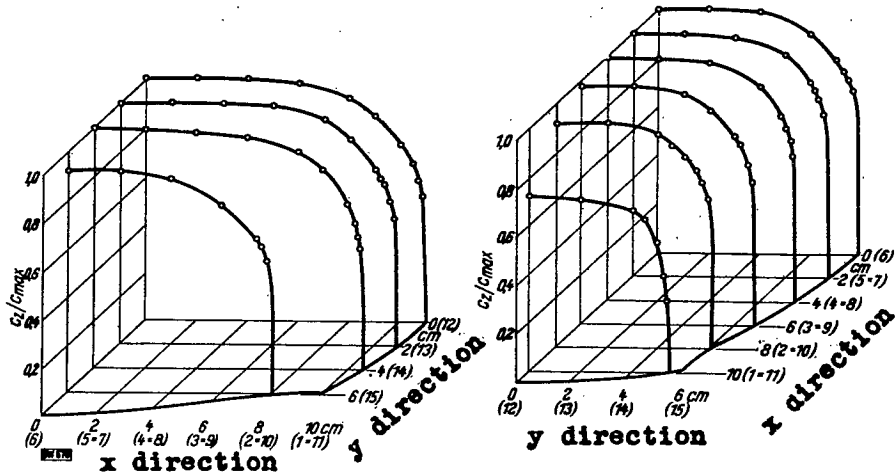
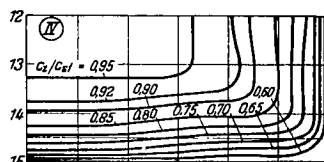
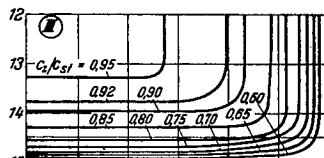
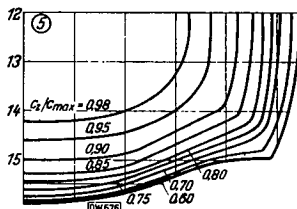
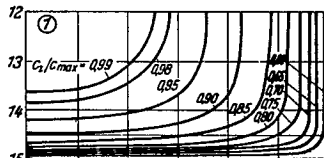
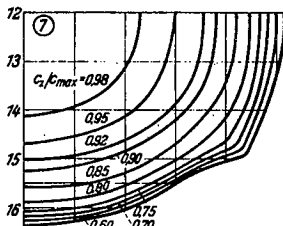
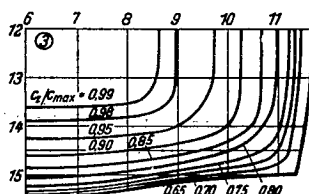
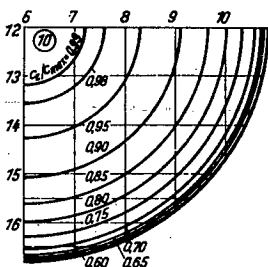
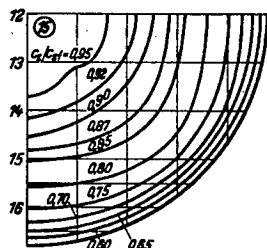
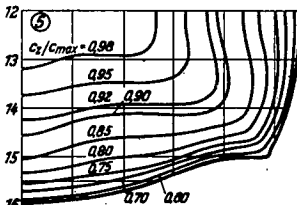
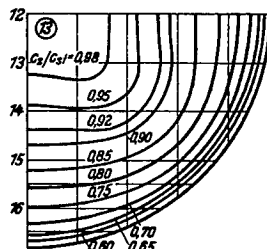
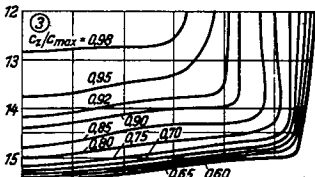
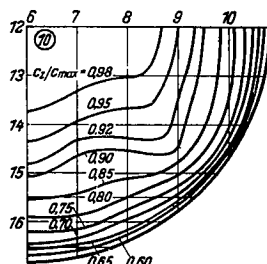
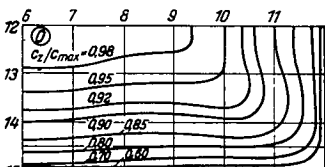


Figure 33.- Velocity distribution (c_z/c_{max}) in the horizontal (x) and vertical (y) measuring planes of cross section 5 of the transition $C \rightarrow R(II)$.



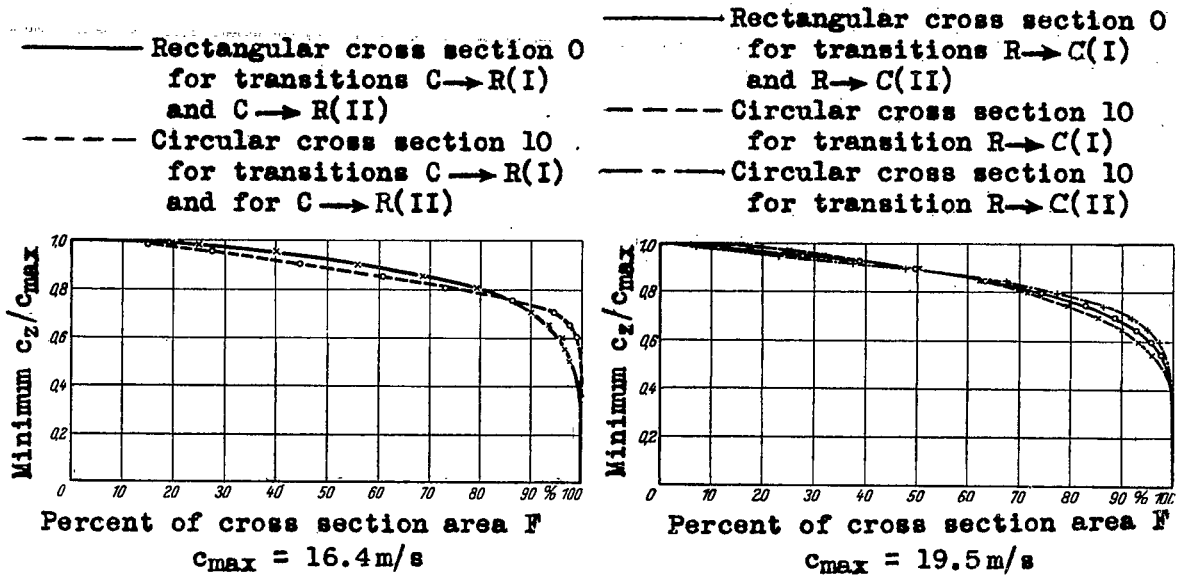
Figures 34-38.- Isotachs in cross sections 10,7,5,3 and 1 of the transition $C \rightarrow R(I)$. Fig. 34 is also for $C \rightarrow R(II)$.

Figures 39,40.- Isotachs in cross sections III and IV of exit run in the transition $C \rightarrow R(I)$.

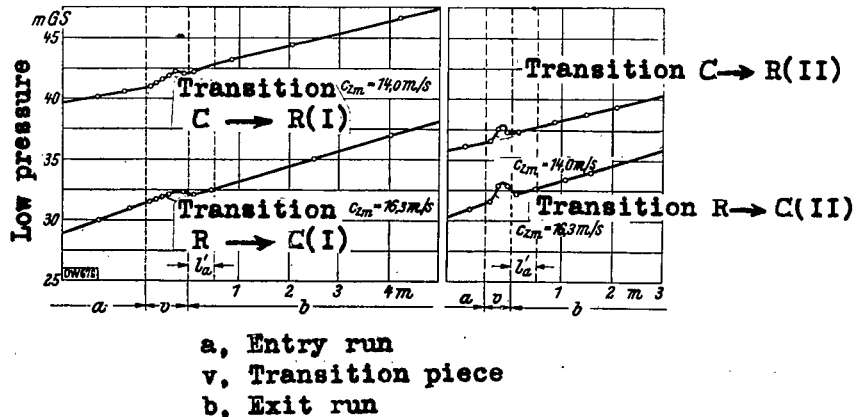


Figures 41-45.- Isotachs in cross sections 0,3,5,7 and 10 of the transition $R \rightarrow C(I)$. Fig. 41 also for $R \rightarrow C(II)$.

Figures 46,47.- Isotachs in cross sections 13, and 15 of exit run for the transition $R \rightarrow C(I)$.



Figures 61,62.- Minimum value of c_z/c_{max} plotted against percent cross section area for sections 0 and 10.



Figures 63,64.- Variation of pressure at the wall along the test length for the various transitions.